

# Metal–Organic Frameworks for Electrocatalysis



Muhammad Usman and Qi-Long Zhu

**Abstract** Metal–organic frameworks (MOFs) have recently become prospective materials for electrocatalysis. MOFs constructed via coordination chemistry of inorganic metal nodes and organic ligands, possess the exclusive features over traditional inorganic or organic materials, which include ultrahigh porosity, large surface areas, structural tunability and high stability. Based on these features, MOFs are already being applied in storage and separation, catalysis, optoelectronics, drug delivery and biomedical imaging. Particularly, with the advantageous feature, MOFs have potential to work as efficient electrocatalysts for a variety of redox reactions, such as hydrogen evolution reaction (HER), oxygen reduction reaction (ORR), oxygen evolution reaction (OER), etc. In this chapter, a discussion has been presented on MOFs, their composites, MOF-derived carbon materials and their performance as electrocatalysts. This chapter will inspire new research direction regarding the development of advanced electrocatalytic materials using MOFs.

**Keywords** Metal–organic frameworks · Coordination polymers · Electrocatalysts · Electrochemistry

## Abbreviations

HER	Hydrogen evolution reaction
OER	Oxygen evolution reaction
ORR	Oxygen reduction reaction
CO <sub>2</sub> RR	Carbon dioxide reduction reaction
MOFs	Metal–organic frameworks
PCPs	Porous coordination polymers
ZIFs	Zeolitic imidazolate frameworks
CPE	Controlled-potential electrolysis

---

M. Usman · Q.-L. Zhu (✉)

State Key Laboratory of Structural Chemistry, Fujian Institute of Research on the Structure of Matter (FJIRSM), Chinese Academy of Sciences (CAS), Fuzhou 350002, China  
e-mail: [qlzhu@fjirsm.ac.cn](mailto:qlzhu@fjirsm.ac.cn)

DMF	Dimethylformamide
DEF	Diethylformamide
GC	Glassy carbon
CV	Cyclic voltammetry
TS	Tafel slope
TON	Turnover number
BHT	Benzenehexathiol
TOF	Turnover frequency
MoS <sub>x</sub>	Molybdenum polysulfide
POMs	Poly oxometalates
OFP	Open-framework polyoxometalate
POMOFs	POM-based metal-organic frameworks
TBA	Tetrabutylammonium ion
BDC	1,4-benzene-dicarboxylate
BTB	Benzenetribenzoate
BTC	1,3,5-benzenetricarboxylate
H <sub>4</sub> dcpa	4,5-di(4'-carboxylphenyl)phthalic acid
azene	( <i>E</i> )-1,2-di(pyridin-4-yl)diazene
4,4'-bpy	4,4'-bipyridine
2,2'-bpy	2,2'-bipyridine
H <sub>2</sub> adip	Adipic acid
5-H <sub>2</sub> bdc	5-nitroisophthalic acid
Im	Imidazolate
mim	2-methylimidazolate
bim	Benzimidazolate
H <sub>2</sub> bbta	1H,5H-benzo(1,2-d:4,5-d')bistriazole
H <sub>2</sub> TCP	4,4',4'',4'''-(porphyrin-5,10,15,20-tetrayl)tetrabenzoate
BHT	Benzenehexathiol
tht	Triphenylene-2,3,6,7,10,11-hexathiolate
HITP	2,3,6,7,10,11-hexaiminotriphenylene
tpy	2,2':6',2''-terpyridine
H <sub>2</sub> dcbpy	2,2'-bipyridine-5,5'-dicarboxylic acid
H <sub>2</sub> bpdc	4,4'-biphenyldicarboxylic acid
ade	Adenine
TBA	Tetrabutylammonium
BPT	[1,1'-biphenyl]-3,4',5-tricarboxylate
trim	1,3,5-benzenetricarboxylate
biphen	4,4'-biphenyldicarboxylate
tbapy	1,3,6,8-tetrakis (p-benzoate) pyrene
Ted	Triethylene-diamine
PB	Phosphate buffer
FTO	Fluorine-doped tin oxide
NF	Nickel foam
NFF	NiFe alloy foam
GO	Graphene oxide

GA	Graphene aerogel
CNTs	Carbon nanotubes
NPs	Nanoparticles
NGO	Nitrogen-doped graphene oxide
DHT	Dihydroxyterephthalate
RDE	Rotating-disk electrode
NCNHP	N-doped carbon hollow polyhedron
LDH	Layered double hydroxide
SURMOF	Surface-mounted metal–organic framework
SURMOFD	Surface-mounted metal–organic frameworks derivative

## 1 Introduction of Metal–Organic Frameworks (MOFs)

Metal–organic frameworks (MOFs) are constructed through coordination bonds via highly organized metal nodes and organic linkers, [1] which results into the formation of highly-order crystalline frameworks with ultrahigh porosity, large surface areas, unique host-guest dynamics, thermal stability and mechanical flexibility, etc. [2]. Owing to these structural and functional properties, MOFs have been widely used for many applications such as storage and separation, water purification, optoelectronics, proton conduction, dielectrics, drug delivery, chemical sensors and biomedical applications [3, 4]. Beside these traditional applications, there is a huge scope for utilization of MOFs into wider industrial applications. Generally, MOFs are constructed through self-assembly of metal nodes/clusters and organic ligands in certain solvents as shown in Fig. 1 [5], forming one-, two- and three-dimensional periodic frameworks with permanent porosity. The structural geometry of MOFs depends upon the coordination numbers and orientation of binding sites of metal and the organic ligands as demonstrated in Fig. 2 [6, 7]. For example, a hexagonal diamondoid network will be formed from linear bifunctional ligands via coordination with metal nodes of tetrahedral geometry. Similarly, a octahedral network will be generated from the metal nodes with octahedral geometry [8].

With their ultrahigh surface areas of more than even  $10,000 \text{ m}^2 \text{ g}^{-1}$  and pore sizes of greater than 10 nm, MOFs are regarded as superior materials than the commercially available porous materials like activated carbon [8–10]. For instance, the isorecticular series of MOF-74, which are constructed with numbers of phenylene rings (I) as linkers, have the pore apertures of up to 98 angstroms (IRMOF74-XI) [11]. There is substantial research on the synthesis of novel MOFs and more than 30,000 MOFs have been reported with a variety of shapes, structures and applications. Some examples of porous MOFs are shown here in Fig. 3 [12].

MOFs possess high surface areas and abundant active sites, which recently expands their applications towards electrochemistry. However, the low charge transfer in MOFs is a big hurdle to use them in electrical energy related applications. MOFs generally have very low conductivity less than  $10^{-10} \text{ S/cm}$  [13]. The low electrical

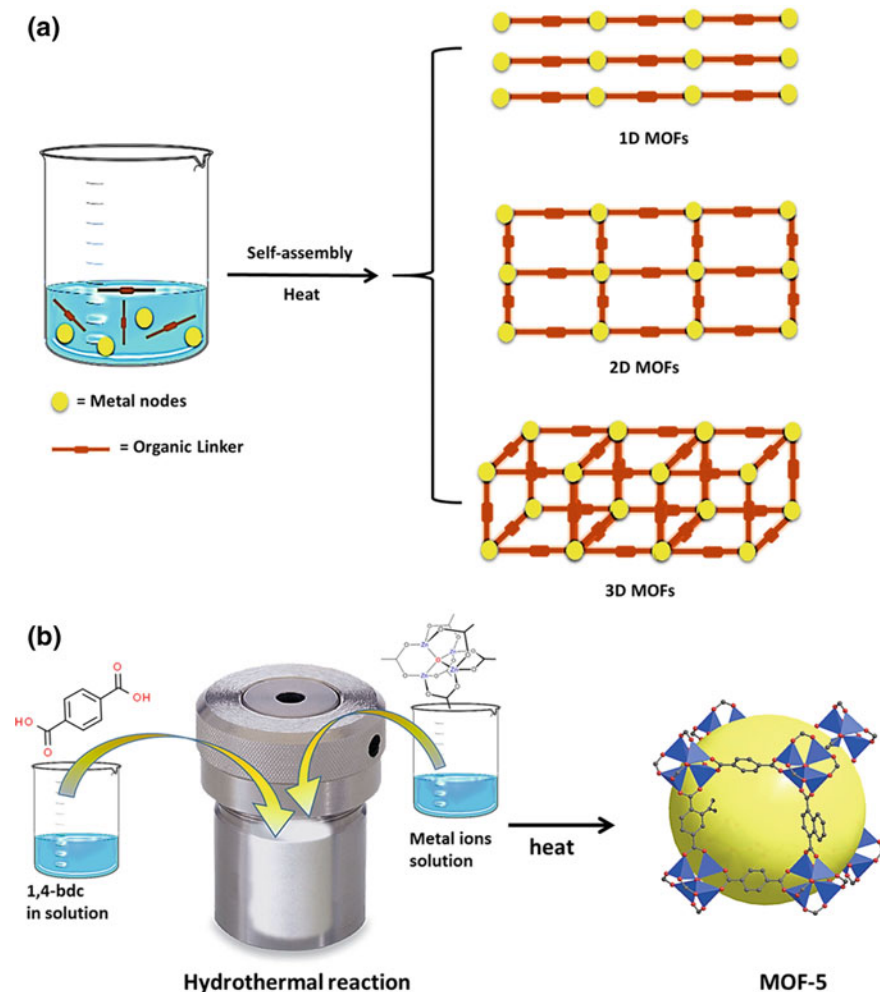


**Fig. 1** **a** Generic scheme for the preparation of 1D, 2D and 3D MOFs. **b** Preparation scheme for MOF-5 via hydrothermal process

conductivity of MOFs is due to maximum use of carboxylic linkers in their synthesis [14]. The electronegativity of the oxygen atom is higher, which requires higher voltage to pass the electrons through the linker. Poor overlap of oxygen with the metal d-orbitals is also responsible for the low charge transfer in MOFs. In addition to their key structural features such as high surface areas, good stability, abundant active sites, it is important to understand charge transfer in MOFs, which will help to expand the applications of MOFs towards electrochemistry. The recent progress of electrically conductive MOFs that can enable the great enhancement in the conductivity for their application in the field of electrocatalysis. Given that the electrical

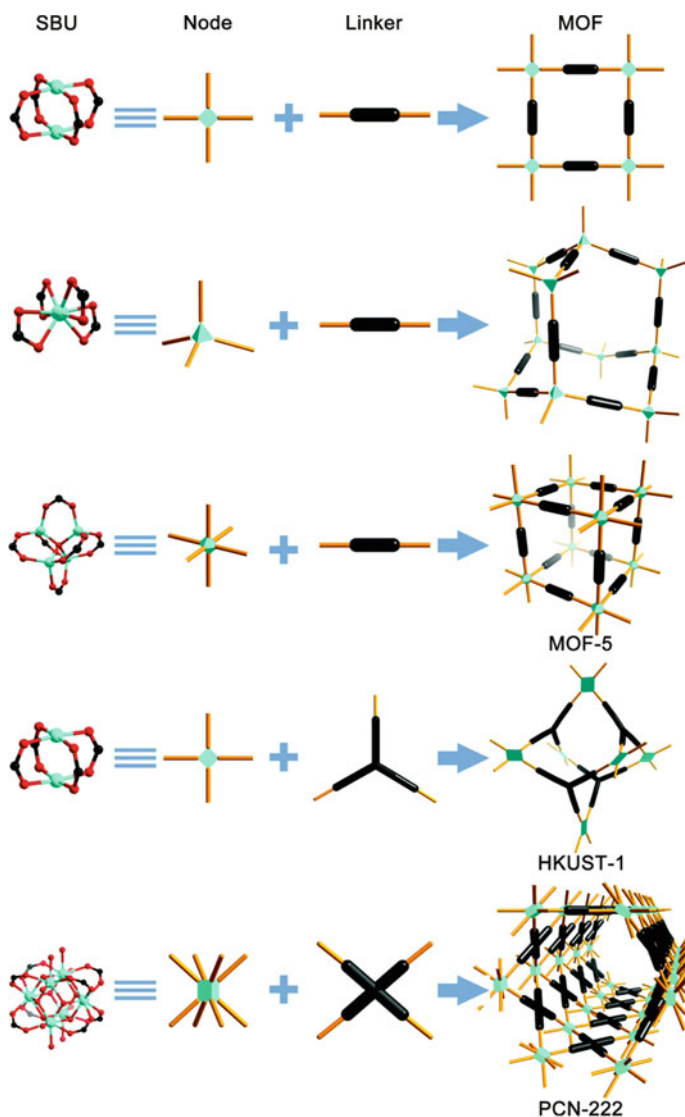


**Fig. 2** Coordination geometries of some representative MOFs from metal nodes and organic linkers [6]. Reprinted with permission from Ref. [6]. Copyright © 2014 Royal Society of Chemistry

properties of the MOFs can be regulated by the structural tunability, post-synthesis modifications, host and guest chemistry within the frameworks, the solvent molecules and their interactions, and the cooperation of conducting molecules/particles, MOFs will offer a promising opportunity for being used as industrially vital energy storage/generation materials. The abundant functionality, high surface areas, ease of tunability of crystal structures, and modification on functional groups mark MOFs

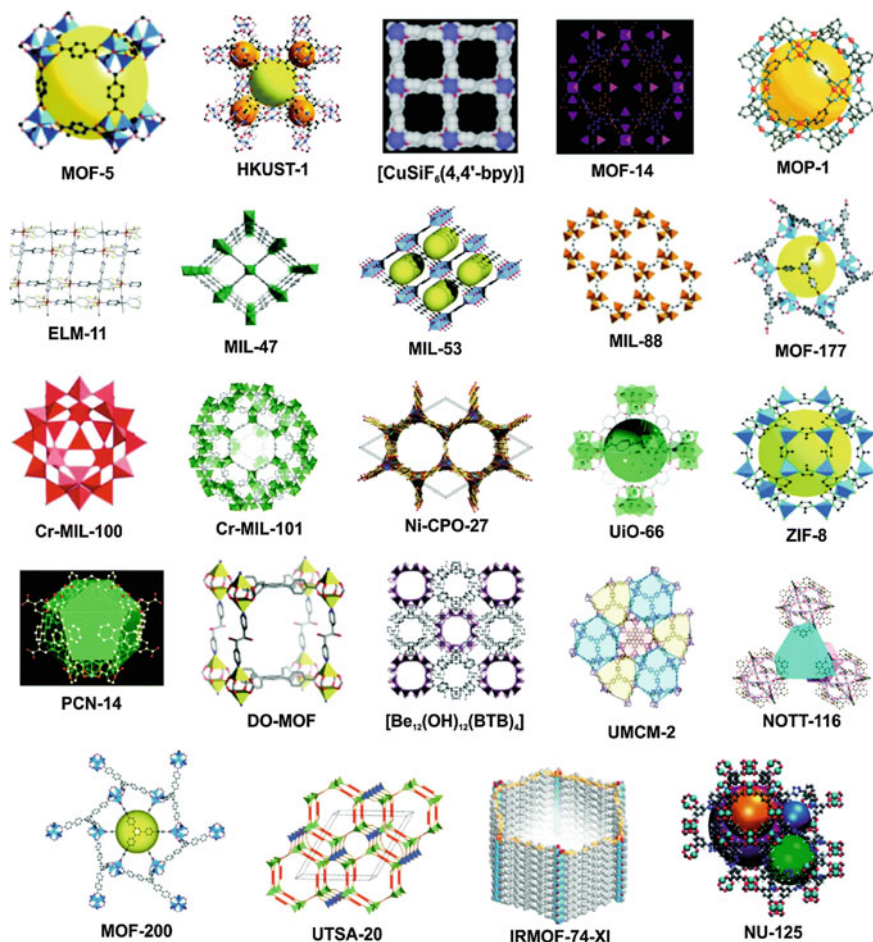


**Fig. 3** Crystal structures of some famous MOFs with high porosity and surface areas [12]. Reprinted with permission from Ref. [12]. Copyright©2015 Royal Society of Chemistry

highly useful as compared with other inorganic and organic materials for designing efficient electrocatalysts. However, the study of the charge transfer behaviors of MOFs is still in its preliminary stage and additional studies will be needed [15, 16]. Scientists have reported on developing MOFs that show intrinsic conductivity. High conductivity was investigated for thin films composed of  $[\text{Ni}_3(2,3,6,7,10,11\text{-hexaiminotriphenylene})_2]$ , which can be utilized as electrocatalysts for ORR [17–20]. Recently, a highly conductive Cu-based MOF  $[\text{Cu}_2(6\text{-Hmna})(6\text{-mn})\cdot\text{NH}_4]_n$  (Hmna = mercaptonicotinic acid, 6-mn = 6-mercaptonicotinate) has been reported, which consists of a 2D  $(\text{Cu-S})_n$  plane and shows conductivity of  $10.96 \text{ S cm}^{-1}$  for its single crystal measurements [21]. Metal centres with the higher charge density (Cu and Fe etc.), electron enriched organic linkers and charge transfer mechanisms could be the

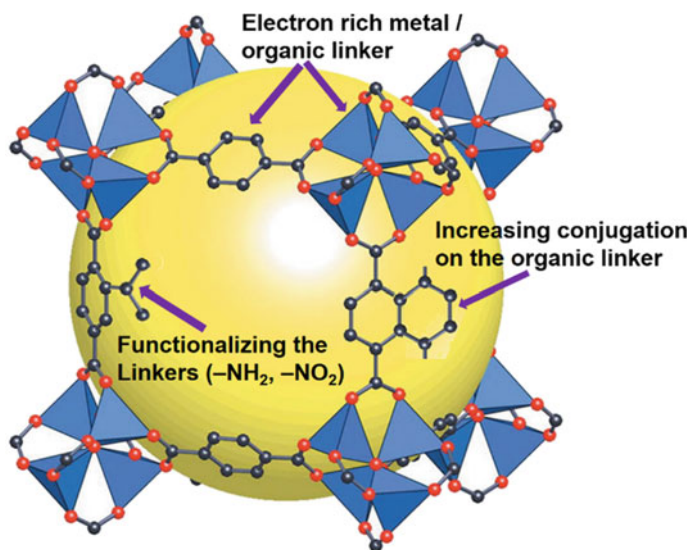


**Fig. 4** Proposed mechanisms for bandgap engineering for MOF-5 with bandgap of 3.4 eV to improve electrical conductivity [16, 22]. Reprinted with permission from Ref. [22]. Copyright©2016 John Wiley and Sons

factors for increasing the electrical conductivity of these MOFs. Therefore, electrical conductivity of MOFs can be improved by three ways as follows: (i) growing the conjugation on the organic molecule, (ii) choosing electron-enrich metals and organic linkers, and (iii) functionalizing organic linkers with nitro, sulfide and amino groups (Fig. 4) [22].

## 2 MOFs for Electrocatalysis

With the increasing consciences on climate change and development of renewable energy sources, the investigation on effectual electrochemistry in electrolytic cells, batteries, supercapacitors, and fuel cells have been accelerated in modern times [23]. Electrochemical devices comprise of various type of electrochemical reactions, including HER, ORR, OER, carbon CO<sub>2</sub>RR, metal ions redox reactions, etc. [24]. However, improving the efficiency and performance of electrochemical devices is a challenging task. Most of devices involving these half reactions need extra potentials to operate due to the slow reaction kinetics of these mechanisms. In efforts to improve the rate of electrochemical reactions, highly efficient and selective catalysts are required and their electrochemical performance is dependent on the sample amount. To meet the requirement of high catalytic activity and selectivity, MOFs with their ultrahigh surface areas and a number of active centers are among the promising candidates for the future of electrocatalysis.

Based on current progress, MOFs can be helpful as electrocatalysts in the process of energy generation with high activity and multi-dimensional designing. Some pristine MOFs have been used as electrocatalysts for different electrocatalytic reactions. However, the electrocatalytic performances of pristine MOFs are sometime limited by their insufficient conductivity. In order to overcome the low charge transfer in porous MOFs, several methods have been adopted such as compositing with inorganic/organic materials, carbonization of MOFs, etc. (Fig. 5) [4, 25, 26]. Particularly, pyrolysis of MOFs to form MOF-derived carbon materials is one of the most successful strategies, where the organic linkers are decomposed to give graphitic carbon materials while metal nodes generate active metal sites in different forms [27]. In this technique, MOFs are regarded as precursors for designing various nanostructures to achieve desired functionality. In this regard, the MOFs with different metals such as Co, Zn and Fe and amino-functionalized ligands are widely used as they can produce heteroatom/metal-doped carbons, which are suitable for catalytic activity [28–30].

Porous MOFs, their composites and MOF-derived materials provide an opportunity for electrochemical applications to improve diverse electrochemical reactions. Recent progresses in exploring MOFs and MOF-based materials as electrocatalysts for HER, ORR, OER, and so on, are discussed in detail in this chapter. Research articles appeared on electrocatalytic MOFs are significantly increasing with every passing years (Chart 1). This chapter provides a literature summary of recent progresses on (i) pristine MOFs as electrocatalysts, (ii) MOF composites as electrocatalysts and (iii) MOF-derived materials as electrocatalysts (Fig. 5).

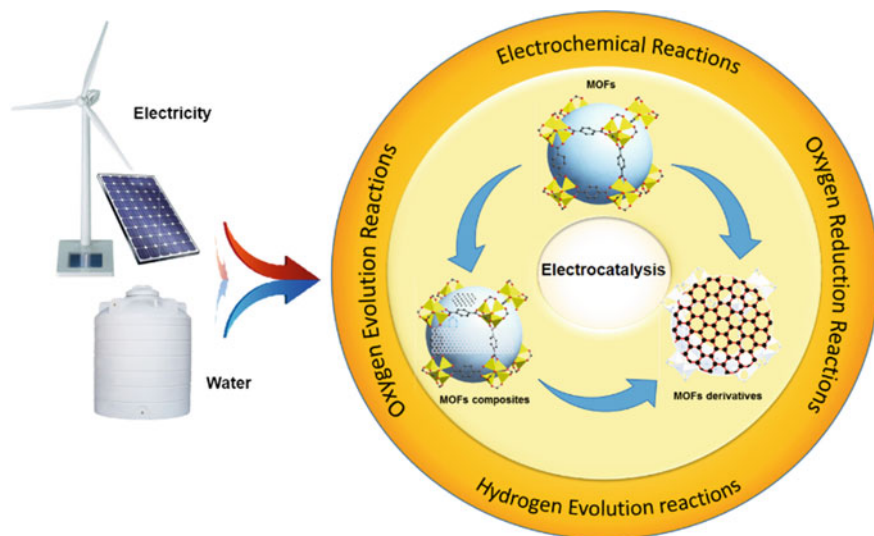
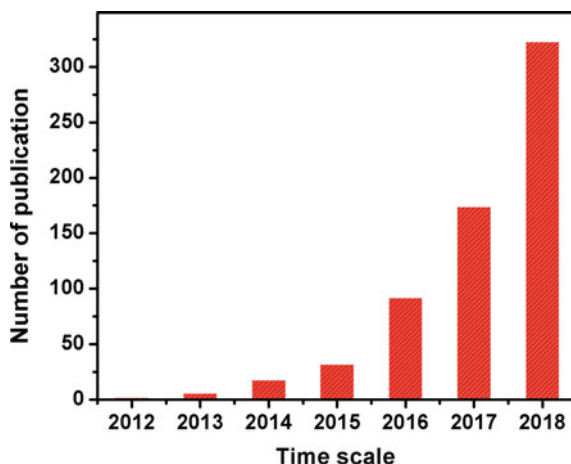


**Fig. 5** MOFs as electrocatalysts are divided into three categories. (i) Pristine MOFs, (ii) MOFs composites, and (iii) MOFs derivatives

**Chart 1** Progress on publications of MOFs and their applications for electrocatalysis with respect to time (data obtained from the ISI Web of Science)



## 2.1 Pristine MOFs as Electrocatalysts

MOFs have been regarded as alternative materials for traditional inorganic 2D and 3D materials for many applications [31]. MOF materials possess heterogeneous nature, better carrier mobility, high stability, and good surface/volume ratio, which allow to use them for electrocatalysis and batteries. With a mass of active metal sites, porous MOFs have been investigated for their electrocatalytic performance for HER, OER, ORR, and other electrochemical reactions. MOF-5,  $[\text{Zn}_4\text{O}(\text{BDC})_3]$ , which is one of the most commonly known MOFs, also called IRMOF-1, was synthesized in ionic liquid system and used as catalyst for HER in 2014 by Liang et al. [32]. Carbon paste electrodes modified with MOF-5(IL) for CV measurements in  $1 \text{ M dm}^{-3} \text{ H}_2\text{SO}_4$  solution indicated that MOF-5(IL) is suitable to catalyze HER. Co-based MOFs, 2D  $[\text{Co}_4\text{L}_2(4,4'\text{-bpy})(\text{H}_2\text{O})_6] \cdot 3.5 \text{ H}_2\text{O}$  and 3D  $[\text{Co}_2(\text{dcpa})(\text{azene})(\text{H}_2\text{O})_3] \cdot \text{DMF}$  constructed with multicarboxylate ligands have also been studied for water splitting, which showed high catalytic performance for the generation of  $\text{H}_2$  as well as  $\text{O}_2$  from  $\text{H}_2\text{O}$  with high current density and low overpotentials [33]. Two Co-based MOFs,  $[\text{Co}(\text{L})_{0.5}(\text{adip})]$  and  $[\text{Co}_2(\text{L})_2(5\text{-bdc})_2(\text{H}_2\text{O})_2 \cdot \text{H}_2\text{O}]$  were founded to exhibit electrocatalytic activities for OER. These MOFs were designed using two ligand system, where the second ligands was 1,4-bis(3-pyridylaminomethyl)benzene (L) [34]. When the MOF-modified electrodes were utilized, a quasi-reversible redox peak with a less potential ( $\eta = 0.46 \text{ V}$ ;  $+1.05 \text{ V}$  vs. SCE) was detected for  $[\text{Co}(\text{L})_{0.5}(\text{adip})]$ , as compared with the water-containing  $[\text{Co}_2(\text{L})_2(5\text{-bdc})_2(\text{H}_2\text{O})_2 \cdot \text{H}_2\text{O}]$  ( $\eta = +0.81 \text{ V}$ ;  $+1.4 \text{ V}$  vs. SCE). Two Co-based MOFs having different coordination bonding of water molecules in the structures were compared based on their HER performance and found that the coordination of solvent molecules in MOF is highly significant to tune the electrocatalytic properties [35].

ZIF series of porous MOFs are well-known for their structural tunability, easy synthesis, and large surface areas, which have structural anatomy similar to Si–O–Si

with angle of  $\theta = 145^\circ$ , leading to the bridges in the form of M–Im–M framework (M = Zn or Co) [36]. High chemical and thermal stability of ZIFs and their structural tunability have potential to produce large number of structures and morphologies to get desired functionality or properties. Post-modifications such as plasma etching on (Co)ZIF-67 can also generate more coordinately unsaturated metal sites in ZIF-67, which improved its electrocatalytic performance [37]. Wang and co-workers have investigated Co-ZIF-9 [Co(bim)<sub>2</sub>] for its OER catalytic activity in a various pH solutions [38]. The theoretical investigation have also been performed using DFT, which revealed that the water was adsorbed firstly at catalyst [Co-ZIF-9], directing H to C atom (C–H = 2.11 Å), and the longer distance of H–O was observed at tradition state while the C–H bond distance was decreased. The DFT study on Co-ZIF-9 revealed that not only active metal site but also the ligands (benzimidazole) played a significant role as proton acceptors during the proton-coupled electron transfer process during OER.

Effect of different metal sites of MOFs on electrocatalytic activity have also been investigated by Wang et al. [39]. A series of isostructural compounds, i.e., a Ni MOF [Ni<sub>3</sub>(btc)<sub>2</sub>(H<sub>2</sub>O)<sub>3</sub>], a Fe MOF [Fe<sub>3</sub>(btc)<sub>2</sub>(H<sub>2</sub>O)<sub>3</sub>] and a mixed metal MOF [Fe<sub>0.23</sub>Ni<sub>2.77</sub>(btc)<sub>2</sub>(H<sub>2</sub>O)<sub>3</sub>], have been synthesized using different metal clusters and their OER performance and alkaline stability were compared (Fig. 6). The thin films of these MOFs have been deposited on Ni foams via electrochemical deposition and it was found that the mix metal compound [Fe<sub>0.23</sub>Ni<sub>2.77</sub>(btc)<sub>2</sub>(H<sub>2</sub>O)<sub>3</sub>] exhibited outstanding OER performance with less overpotential of  $\eta_{10} = 270$  mV and higher current density, as compared with other mononuclear counterparts in their study.

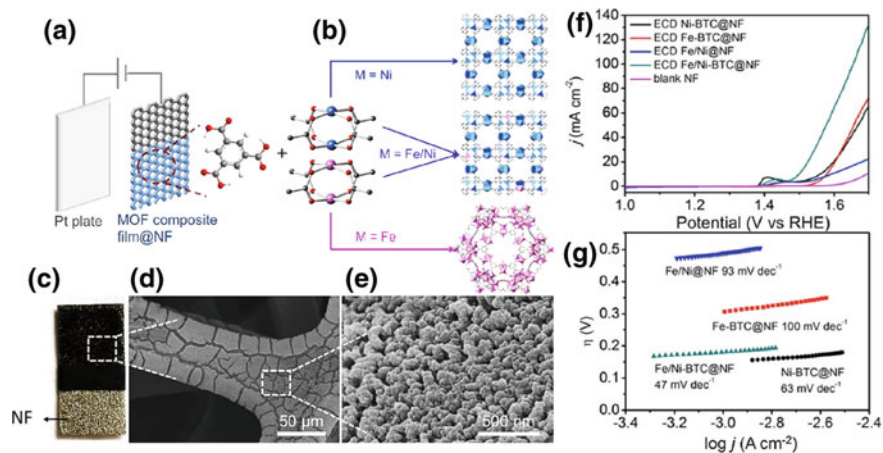


**Fig. 6** a electrochemical setup with two electrodes having MOF deposited on nikal foam and Pt. b Synthetic scheme and crystal structures of [M(btc)<sub>2</sub>] (M = Fe<sub>3</sub>, Ni<sub>3</sub> and Fe<sub>0.23</sub>Ni<sub>2.77</sub>). c Optical and (d, e) SEM images of Fe/Ni-BTC@NF. f Linear sweep voltammetry data and g Tafel plots for [M(btc)<sub>2</sub>] measured at 1 mV s<sup>-1</sup>. Reprinted with permission from Ref. [39]. Copyright 2016@American Chemical Society

Su and coworkers have also reported the crystal engineering of a Fe and Co containing electrocatalytic MOF to achieve excellent OER activity [40]. Strong binding interactions among the catalyst and adsorbate in the bimetallic MOFs as compared with monometallic MOFs resulted in the better catalytic performance of the bimetallic MOFs. Series of bimetallic MOFs have been reported, which exhibited much better electrocatalytic performance over the isostructural monometallic MOFs [41, 42]. Beside bimetallic electrocatalytic MOFs, there are also trimetallic MOFs (e.g., Fe/Ni/Co(Mn)-MIL-53), which exhibited excellent OER activity at an optimized composition of metals [43].

Chen and coworkers reported a Co-based MOF,  $[\text{Co}_2(\mu\text{-OH})_2(\text{bbta})]$  (MAF-X27-OH), which exhibited excellent performance as inorganic OER catalysts with an overpotential  $\eta_{10} = 292$  mV in basic solution (Fig. 7) [44]. In addition, MAF-X27-Cl showed excellent chemical stability in 0.001 M HCl as well as 1.0 M KOH solution for a period of 7 days. It was found that the active metal sites and hydroxide ligands in the MOF played significant role in creating low-energy intraframework coupling pathways.

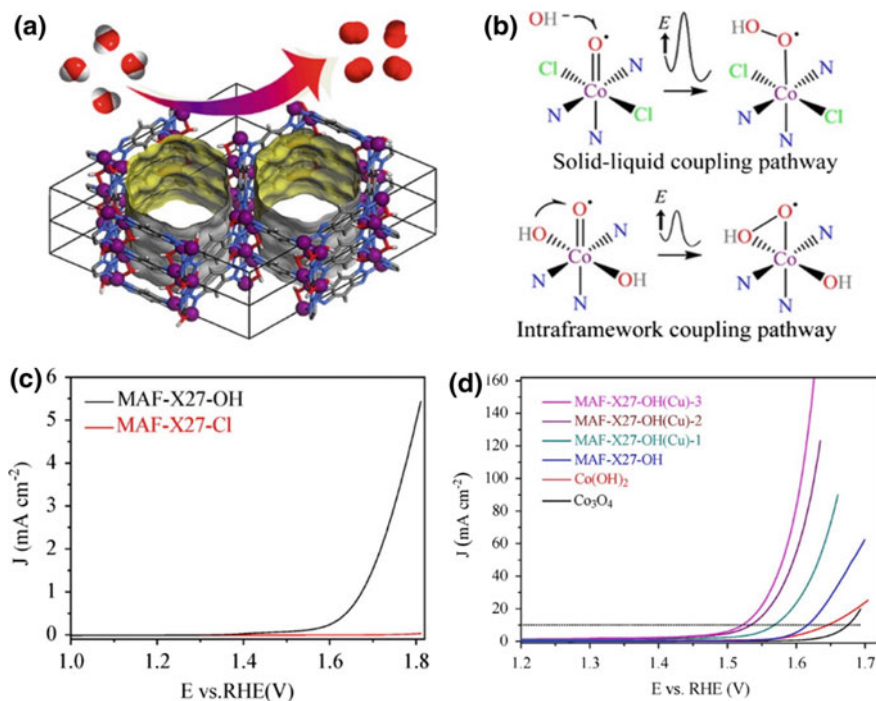


**Fig. 7** **a** Crystal structure of a 3D MAF-X27-OH. **b** Solid–liquid and Intraframework coupling pathways. **c** Linear sweep voltammetry curves in neutral solution. **d** Linear sweep voltammetry plots for different samples and their comparison at pH = 10. Reprinted with permission from Ref. [44]. Copyright 2016@American Chemical Society

Mao and coworkers have designed Cu-BTC and Cu-bipy-BTC, and reported their electrocatalytic properties [45]. This study indicated that these Cu-based MOFs were useful in catalyzing ORR via four-electron reduction pathways. Cu-MOF-modified glassy carbon (GC) electrodes have been designed and their cyclic voltammetry (CV) data were recorded in 0.10 M phosphate buffer solution. Redox reactions of Cu(II/I) in these MOF resulted in electrochemical activity with well-defined redox peaks at a potential of  $-0.10$  V versus Ag/AgCl. The electrocatalytic behavior of Cu-bipy-BTC modified electrode for ORR was much stable as compared with Cu-BTC modified one. Considering the stability issue, a highly robust heterogeneous catalyst PCN223-Fe was designed via reaction of Zr6 oxo clusters and Fe(III) porphyrin ligand and the resulted product was grown on a conductive FTO substrate, which was further utilized as working electrode for ORR in 0.1 M LiClO<sub>4</sub>/DMF [46]. A bifunctional catalytic Fe-based MOF has also been prepared by Yin and coworkers, which not only showed excellent ORR but also displayed remarkable activity for OER in an alkaline solution [47]. The catalytic process adopted a two electron pathway at potentials from  $-0.30$  to  $-0.50$  V versus Ag/AgCl and then shifted to four-electron pathway from  $-0.50$  to  $-0.95$  V versus Ag/AgCl.

Due to the conducting nature of Cu ions, Cu-based MOFs have also been widely reported for electrocatalytic HER, OER and ORR. In addition, there are some MOFs that are reported for electrocatalytic CO<sub>2</sub>RR. [Cu<sub>3</sub>(btc)<sub>2</sub>(H<sub>2</sub>O)<sub>3</sub>] and [Cu<sub>2</sub>(ade)<sub>2</sub>((CH<sub>3</sub>)<sub>2</sub>COO)<sub>2</sub>] have been studied as effective catalysts for CO<sub>2</sub>RR to MeOH and EtOH in bicarbonates [48]. A porphyrin-based MOF [Al<sub>2</sub>(OH)<sub>2</sub>Co-TCPP] has also shown outstanding catalytic properties for CO<sub>2</sub> reduction to CO in aqueous electrolytes with CO selectivity of 76%, TON of 1400 and stable electrolysis for 7 h [49].

Most of the MOFs reported for high porosity possess 3D crystal structures. However, 2D MOFs have the following advantages over traditional electrocatalysts and 3D MOF electrocatalysts. (i) They possess uniform arrangement of the active sites in hexagonal networks; (ii) catalytically active centers can be more exposed in 2D MOFs; (iii) these catalytic active sites can remain active in aqueous solutions due their immobilization with solid-state materials. In order to utilize 2D MOFs for the reduction of water, Marinescu and coworkers have reported on the formation of 2D cobalt dithiolene films (MOS-1 and MOS-2) using bht, a trinucleating conjugated ligand, and cobalt(II) salt via a liquid–liquid interfacial method [50]. MOS-1 [H<sub>3</sub>(Co<sup>III</sup>(bht)<sub>2</sub>)] and MOS-2 [H<sub>3</sub>(Co<sup>III</sup>(tht)<sub>2</sub>)] showed excellent HER performance with maximum conductivity ( $\sigma = 10^{-6}$  S cm<sup>-1</sup>) for MOS-1 (Fig. 8). Square planar coordination geometry of 2-connected metal nodes and 3-connected organic linkers results into the formation of honeycomb-like 2D sheets with a thickness of 360 nm. When the pH value of the buffer solution decreased, the current intensity tended to increase. Under aqueous conditions with a very low value of pH = 1.3, the MOS-1 and MOS-2 electrodes showed the overpotentials of  $\eta_{10} = 0.34$  and 0.53 V, respectively (Fig. 8e, f). Similarly, 2D supramolecular nickel bis(dithiolene) complexes in the form of layered sheets (0.7–0.9 nm) has also been reported for their outstanding electrocatalytic activities for HER with  $\eta_{10}$  of 333 mV and Tafel slope of 80.5 mV dec<sup>-1</sup> [51]. [Ni<sub>3</sub>(HITP)<sub>2</sub>] is a well-known conducting MOF, which is

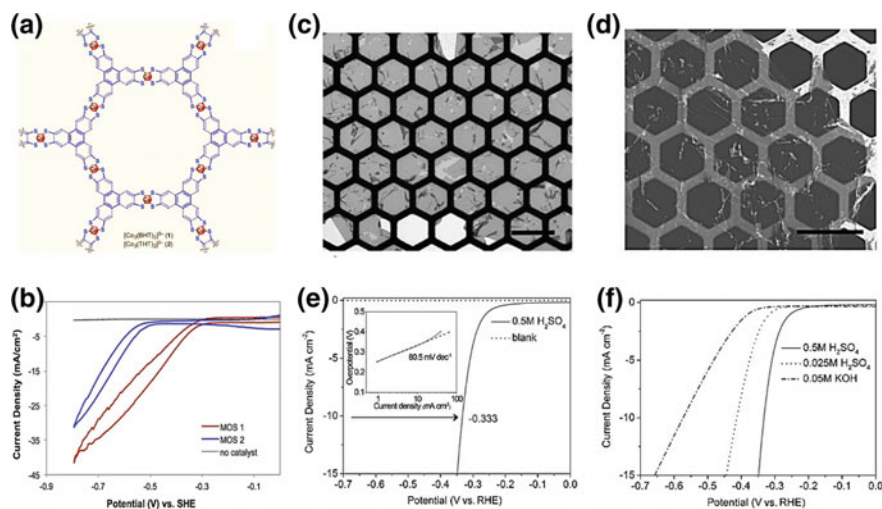


**Fig. 8** **a** A schematic design of the honeycomb-like net of cobalt dithiolenes frameworks. **b** Polarization data of MOS-1, MOS-2 and the blank samples in  $\text{H}_2\text{SO}_4$  solution ( $\text{pH} = 1.3$ ) at scan rate of  $100 \text{ mV s}^{-1}$ . Reprinted with permission from Ref. [51]. Copyright©2015 John Wiley and Sons. **c** TEM and **d** SEM images of layered-sheets of nickel bis(dithiolenes) compounds. **e** Linear sweep voltammetry curves of nickel bis(dithiolenes)-coated electrodes and blank GC-RDE in  $0.5 \text{ M H}_2\text{SO}_4$  solution (Tafel plot ( $80.5 \text{ mV dec}^{-1}$ ) is shown in inset). **f** Polarization curves in different concentration of acidic and basic solutions ( $\text{H}_2\text{SO}_4$  and  $\text{KOH}$ ) at  $10 \text{ mV}^{-1}$  scan rate. Reprinted with permission from Ref. [50]. Copyright©2015 American Chemical Society

among the highest electrical conductive MOFs. Owing to a number of the highly active square planar  $\text{Ni-N}_4$  sites, it has been recently reported for its functions as a tunable electrocatalyst for ORR in alkaline solution, with a  $\eta_{10}$  of  $0.18 \text{ V}$  and good stability [20].

In short, the exposed electrocatalytic active sites and high active site density endow 2D and 3D MOFs with efficient activities for electrocatalysis. Recently reported pristine MOFs as electrocatalysts for HER, OER and ORR are listed in Table 1.

## 2.2 MOF Composites as Electrocatalysts

### 2.2.1 Molecular Catalyst@MOF Composites

With advantage of the highly porous structures of MOFs, catalytically active molecules could be integrated into the pores of MOFs to form novel catalysts, which possess the properties of heterogeneous MOFs and the catalytic properties of the guest molecules. The high exposure of active sites owing to the large surface areas of MOFs could lead to high catalytic activity and stability. A MOF composite

**Table 1** Examples of pristine MOFs as electrocatalysts for HER, OER and ORR

MOFs	Short names	Electrochemical reactions (electrolyte)	$\eta_{10}$ (mV) versus RHE	TS (mV dec <sup>-1</sup> )	References
Na <sub>3</sub> [Co <sub>3</sub> (bht) <sub>2</sub> ]	MOS-1	HER (0.05 M H <sub>2</sub> SO <sub>4</sub> )	340	NA	[50]
H <sub>3</sub> [Co <sub>3</sub> (tht) <sub>2</sub> ]	MOS-2	HER (0.05 M H <sub>2</sub> SO <sub>4</sub> )	530	NA	[50]
H <sub>3</sub> [Ni <sub>3</sub> (tht) <sub>2</sub> ][Cal]	THT-Ni	HER (0.5 M H <sub>2</sub> SO <sub>4</sub> )	333	80.5	[51]
H <sub>3</sub> [Co <sub>3</sub> (tht)(tha)][Cal]	THTA-Co single-layer	HER (0.5 M H <sub>2</sub> SO <sub>4</sub> )	283.0 ± 1.5	71.0 ± 1.1	[52]
H <sub>3</sub> [Co <sub>3</sub> (tht)(tha)][Cal]	THTA-Co	HER (0.5 M H <sub>2</sub> SO <sub>4</sub> )	332.0 ± 1.8	87.0 ± 1.1	[52]
H <sub>3</sub> [Ni <sub>3</sub> (tht)(tha)][Cal]	THTA-Ni single-layer	HER (0.5 M H <sub>2</sub> SO <sub>4</sub> )	315.0 ± 1.7	76.0 ± 1.0	[52]
H <sub>3</sub> [Co <sub>3</sub> (tht) <sub>2</sub> ]	THT-Co single-layer	HER (0.5 M H <sub>2</sub> SO <sub>4</sub> )	323.0 ± 2.0	82.0 ± 1.2	[52]
H <sub>3</sub> [Co <sub>3</sub> (tht) <sub>2</sub> ]	THT-Co	HER (0.5 M H <sub>2</sub> SO <sub>4</sub> )	495.0 ± 1.8	157 ± 1.2	[52]
[Cu <sub>3</sub> (btc) <sub>2</sub> (H <sub>2</sub> O) <sub>3</sub> ]	HKUST-1	HER (0.5 M H <sub>2</sub> SO <sub>4</sub> )	691	127	[53]
[Co <sub>2</sub> (μ-OH) <sub>2</sub> (bta)]	MAF-X27-OH	OER (1 M KOH)	387	66	[44]
[Co <sub>2</sub> (μ-OH) <sub>2</sub> (bta)]	MAF-X27-OH	OER (1 M KOH)	292	88	[44]
[K(H <sub>2</sub> O) <sub>2</sub> Co <sub>3</sub> (cit)(Hcit)]	USTA-16	OER (1 M KOH)	408	77	[54]
[Co(bim) <sub>2</sub> ]	Co-ZIF-9	OER (0.1 M KOH)	510 (1 mA cm <sup>-2</sup> )	93	[38]
[Fe <sub>0.23</sub> Ni <sub>2.77</sub> (btc) <sub>2</sub> ]	Ni/Fe-BTC	OER (0.1 M KOH)	270	43	[39]
[Co(bdc)]	CoBDC	OER (0.1 M KOH)	490	48.8	[55]
[Co(mim) <sub>2</sub> ]	ZIF-67	OER (0.1 M KOH)	443 (4 mA cm <sup>-2</sup> )	NA	[56]
[Co(mim) <sub>2</sub> ]	ZIF-67	OER (0.1 M KOH)	450	102	[57]
[Co <sub>2</sub> (μ-OH) <sub>2</sub> (bta)]	MAF-X27-OH	OER (1.0 M PB)	489	127	[44]

(continued)

Table 1 (continued)

MOFs	Short names	Electrochemical reactions (electrolyte)	$\eta_{10}$ (mV) versus RHE	TS (mV dec <sup>-1</sup> )	References
[Co <sub>2</sub> (dobdc)(H <sub>2</sub> O) <sub>2</sub> ]	MOF-74-Co	OER (0.1 M PB)	492	129	[58]
[Co(mim) <sub>2</sub> ]	ZIF-67	OER (0.1 M PB)	525	125	[58]
[Co(mim) <sub>2</sub> ]	ZIF-67	OER (0.1 M PB)	581	NA	[56]
[Co <sub>2</sub> (ptbc) <sub>4</sub> ]	NA	OER (0.2 M PB)	671	NA	[59]
[Pb <sub>2</sub> (H <sub>2</sub> tcpp)]	PbTCPP	OER (0.2 M PB)	NA	126	[60]
[Cu <sub>2</sub> (OH)(bpy) <sub>2</sub> (btc) <sub>3</sub> ]	NA	ORR (0.1 M PB)	3.8 (0.40 V)	NA	[45]
[Al <sub>2</sub> (OH) <sub>2</sub> (Co(tcpp))]	Co-Al-PMOF	ORR (0.1 M H <sub>2</sub> SO <sub>4</sub> )	2.9 (0.55 V)	NA	[61]
[Zr <sub>6</sub> (μ <sub>3</sub> -O) <sub>4</sub> (μ <sub>3</sub> -OH) <sub>4</sub> (Fe(tcpp)) <sub>3</sub> Cl <sub>3</sub> ]	PCN-223-Fe	ORR (DMF)	3.2 (−0.65 vs. SHE)	NA	[46]
[Ni <sub>3</sub> (tha) <sub>2</sub> ]	NA	ORR (0.1 M KOH)	2.25 (0.77 V)	−128	[20]
[Cu <sub>3</sub> (bic) <sub>2</sub> (H <sub>2</sub> O) <sub>3</sub> ]	HKUST-1	ORR (0.1 KOH)	1.74 (0.77 V)	NA	[62]
[Co(mim) <sub>2</sub> ]	ZIF-67	ORR (0.1 M KOH)	NA	−50	[57]
[Fe <sub>3</sub> F(H <sub>2</sub> O) <sub>2</sub> O(btc) <sub>2</sub> ]	MIL-100(Fe)	ORR (0.1 M KOH)	2.1 (0.47 V)	−137	[47]
[Cr <sub>3</sub> F(H <sub>2</sub> O) <sub>2</sub> O(btc) <sub>2</sub> ]:[Co(salen)]	Co-salen@MIL-100(Cr)	ORR (0.1 M PB)	3.84	NA	[63]

(MoS<sub>x</sub>)<sub>y</sub>/UiO-66-NH<sub>2</sub> (y = 1–6) has been reported where the HER activity of molybdenum polysulfide (MoS<sub>x</sub>) combined high chemical stability of UiO-66-NH<sub>2</sub> resulted in novel HER catalysts [64]. MOF composite with MoS<sub>x</sub> exhibited excellent HER activity with  $E_{\text{onset}} = 125$  mV, Tafel slope = 59 mV dec<sup>-1</sup>,  $\eta_{10} = 200$  mV and TOF = 1.28 s<sup>-1</sup>. It was highly stable even after 5000 cycles of CV. Dong and coworkers have synthesized a series of 2D MOFs and furthermore the metal dithiolene-diamine (MS<sub>2</sub>N<sub>2</sub>), metal bis(dithiolene) (MS<sub>4</sub>), and metal bis(diamine) (MN<sub>4</sub>) complexes were integrated into the hexagonal networks of these 2D MOFs [52]. These highly active molecular sites in the 2D MOFs are suitable for electrocatalytic H<sub>2</sub> production. It can be seen that the catalytic activities of the complexes followed by the order of CoS<sub>2</sub>N<sub>2</sub> > NiS<sub>2</sub>N<sub>2</sub> > CoS<sub>4</sub> and the protonation step took place at the M–N sites of the MS<sub>2</sub>N<sub>2</sub> based compounds. Hence, highly order arrangement of the active sites is highly important to deliver the electrocatalytic performance.

Integration of electrocatalytic metal-containing molecules into the pores of the MOFs is a quite successful technique, which can balance the charge in the MOFs via redox hopping and support to get desired catalytic properties. Combining the catalytic activity of metal complexes with advantageous properties of MOFs can be useful for high performance electrocatalysis. A molecular water oxidation catalyst, [Ru(tpy)(dcbpy)(OH<sub>2</sub>)](ClO<sub>4</sub>)<sub>2</sub>, has been integrated into the well-known porous MOF, [Zr<sub>6</sub>O<sub>4</sub>(OH)<sub>4</sub>(bpdc)<sub>6</sub>] (UiO-67), grown on the surface of FTO, by post-synthetic ligand exchange (Fig. 9) [65]. The resulting UiO-67-[RuOH<sub>2</sub>]@FTO as a new OER electrocatalyst can oxidize water at 1.5 V versus Ag/AgCl with a current density of 11.5  $\mu\text{A cm}^{-2}$ . It was found that the intrinsic UiO-67 show poor OER activity ( $\eta = 766$  mV at a current density of 0.05 mA cm<sup>-2</sup>, pH = 8.4); however, after integration of the Ru-complex into this MOF, the current density was enhanced to 0.5 mA cm<sup>-2</sup> at  $\eta = 766$  mV (Fig. 9). This study also indicates that the MOF supports are able to stabilize the structure of Ru-based catalysts. Then, a similar result was reported in 2016, where Ru(tpy)(dcbpy)OH<sub>2</sub>]<sup>2+</sup> has been integrated to thin films of UiO-67 to form the Ru-UiO-67 electrocatalyst, which oxidized H<sub>2</sub>O with a TOF of 0.2 ± 0.1 s<sup>-1</sup> at 1.71 V versus NHE in solution of pH = 7 [66].

MOF-based composite [Cr<sub>3</sub>F(H<sub>2</sub>O)<sub>2</sub>O(BTC)<sub>2</sub>]-[Co(salen)] (Cr-MIL-100-Co-salen) has also been reported for its excellent ORR performance. The composite consist of highly porous Cr-MIL-100 and a Co(II) complex [63]. The 3D Cr-MIL-100, with the pore window diameters of 4.8 × 5.8 Å<sup>2</sup> and 8.6 × 8.6 Å<sup>2</sup> and incredibly large internal pores (25 and 29 Å), can incorporate Co-salen (15.3 × 9.2 × 5.0 Å<sup>3</sup>) inside its pores via the synthetic approach called “ship in a bottle”. GC electrode modified Co-salen@Cr-MIL-100 has been investigated for the ORR performance in PB electrolyte of pH = 6.84. The results of CV indicated sharp peak at potential of 0.39 V versus RHE, which was assigned to O<sub>2</sub> reduction. The composite had good reproducibility of CV data for 50 cycles and was stable for 24 h in a buffer solution of pH = 7.

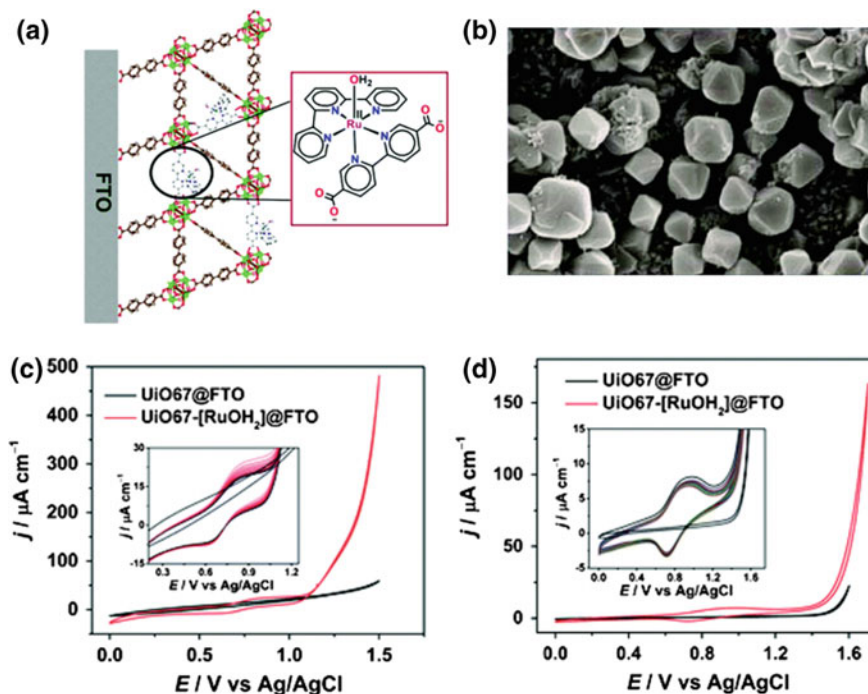


**Fig. 9** **a** Representation of Ru-UiO-67 deposited on FTO electrode and its symmetric unit. **b** SEM image of Ru-UiO-67. CV plots of UiO-67 and Ru-UiO-67@FTO in **c** pH = 8.4 and **d** pH = 6.2. Region of the RuIII/II coupling is shown in **c**, **d**. Reprinted with permission from Ref. [65]. Copyright©2017 Royal Society of Chemistry

### 2.2.2 POM@MOF Composites

Anionic metal-oxide clusters of metals from d-block, called polyoxometalates (POMs) are emerged as novel multifunctional materials with advantageous electrocatalytic properties [67]. Incorporation of POMs into highly porous MOFs with high surface areas can greatly increase the dispersion of POMs. In addition, high thermal stability, recyclability and easy structural tunability are the significant advantages of POM-based MOF materials as heterogeneous catalysts with enriched catalytic properties. Three different types of POM@MOF composite materials can be prepared which includes (i) POMs as nodes directly connecting with organic linkers, (ii) POMs inside the pores of MOFs and (iii) porous POM-pillared coordination polymers (Fig. 10a).

There are several reports on POM-based MOFs for the electrochemical applications particularly for HER [51, 52, 68, 69]. Dolbecq and coworkers presented that MOFs constituted using POMs could inherit catalytic properties of POMs and will be useful for electrochemical reactions [68]. They reported the designing of a POM-based MOF using  $\epsilon$ -Keggin Zn building blocks. It was found that the POM-based

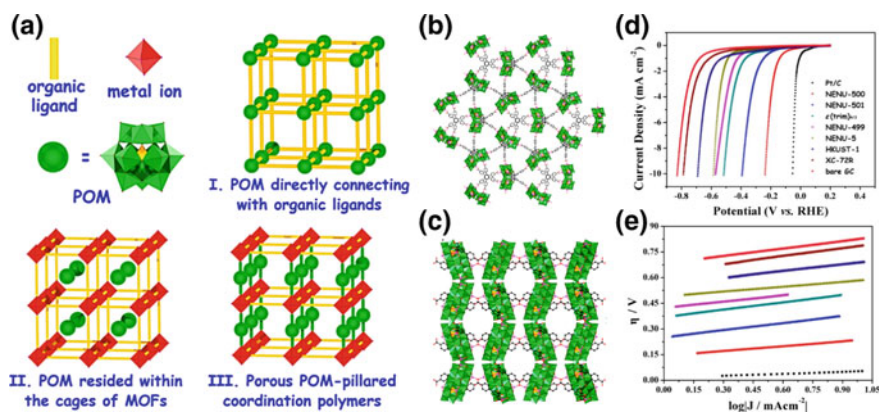


**Fig. 10** a Possible construction of different types of POM@MOF composites. b Crystal structure of (b) NENU-500 and (c) NENU-501. c Comparison of linear sweep voltammetry plots of different materials. d Tafel plots for NENU-500, NENU-501 and related compounds after coating on electrodes in acidic solution. Reprinted with permission from Ref. [53]. Copyright@2015 American Chemical Society

materials displayed excellent catalytic behavior for HER with a high TOF ( $6.7 \text{ s}^{-1}$ ) at  $\eta = 200 \text{ mV}$  in aqueous solution. CPE measurements at  $E = -0.2 \text{ V}$  versus RHE indicated 95% higher FE and a large TOF ( $6.7 \text{ s}^{-1}$ ). Bonding the redox activity of POMs and porous MOFs, Lan, Zhou and coworkers have also reported the POM-based MOFs, NENU-500 ( $[\text{TBA}]_3[\epsilon\text{-PMo}_8^{\text{V}}\text{Mo}_4^{\text{VI}}\text{O}_{36}(\text{OH})_4\text{Zn}_4][\text{BTB}]_{4/3}\cdot x\text{Guest}$ ) and NENU-501 ( $[\text{TBA}]_3[\epsilon\text{-PMo}_8^{\text{V}}\text{Mo}_4^{\text{VI}}\text{O}_{37}(\text{OH})_3\text{Zn}_4][\text{BPT}]$ ), as efficient electrocatalysts for HER (Fig. 10b–e) [53]. NENU-500 exhibited outstanding performance for HER in acidic solution (Fig. 10d, e). Owing to its high stability, large porosity, and abundant active sites, NENU-500 is recognized for its best electrocatalytic performance for HER performance among all MOFs. The current studies on POM-based MOFs demonstrate that with high porosity and stability, these materials have a lot of opportunities as hydrogen-evolving electrocatalysts with outstanding activity.

Mixed-valent  $[\epsilon\text{-PMo}_8^{\text{V}}\text{Mo}_4^{\text{VI}}\text{O}_{40}\text{Zn}_4]$  ( $\epsilon\text{Zn}$ ) Keggin units have also been reported for their HER catalytic performance [70]. The POM-based MOFs were designed using metallic cations  $[\text{M}(\text{bpy})_3]^{2+}$  ( $\text{M} = \text{Co}, \text{Ru}$ ) and tritopic/ditopic organic linkers. Their electrocatalytic HER performance was measured in  $0.1 \text{ M H}_2\text{SO}_4$  ( $\text{pH} = 1.0$ ) aqueous solution. Reduction of protons was found to be responsible for this catalytic activity at potentials below  $-0.6 \text{ V}$  versus Ag/AgCl. From this study, it can be concluded that the existence of monovalent cations such as  $\text{TBA}^+$  or  $\text{PPh}_4^+$  in POM-based MOFs resulted in better catalytic properties of these compounds as compared with the bigger divalent counterions like  $[\text{M}(\text{bpy})_3]^{2+}$  ( $\text{M} = \text{Ru}, \text{Co}$ ). However, the dimension of crystal structure and the nature of POM unit did not affect much on electrocatalytic properties.

### 2.2.3 Graphene/Carbon@MOF Composites

MOFs are known as low conducting materials; hence, to overcome this disadvantage of MOFs, researcher have designed their composite with highly conducting materials such as graphene, which can improve the conductivity of MOFs and further expand their applications as electrocatalysts. In efforts to enhance the conductivity of pristine MOFs, a Cu-MOF composite with GO, (GO X wt%) Cu-MOF, was reported as catalyst for HER, OER and ORR. The catalytic activity of the composite materials with various GO weight% in the MOF was investigated [71]. The Cu-MOF composite with 8 wt% GO exhibited excellent catalytic performance for different electrochemical reactions and better stability in acid media as compare to intrinsic MOF.

Nitrogen doped graphene and other carbon materials with their high electrical conductivity are well-known for non-Pt-based ORR catalysts [72]. Combining their high conductivity feature with porosity of MOFs is quite successful for improving electrocatalytic properties. Hence, the ZIF-67/N-doped carbon composites in different ratios have been investigated for ORR performance in 0.1 M KOH with  $n$  value of  $\sim 4$  (0.55 V vs. RHE). CPE indicated that the ZIF-67/N-doped carbon with 2:1 ratio have good stability for more than 10,000 s [57].

### 2.2.4 Metal-Based NP@MOF Composites

MOFs with a large number of nanopores can also be used as templates for hosting metal-based NPs [73, 74], which could be used as efficient electrocatalysts [75]. Hupp and coworkers presented NU-1000 ( $[\text{Zr}_6(\mu_3\text{-OH})_8(\text{OH})_8(\text{tbapy})_2]$ ) as scaffolds for designing Ni–S rods with higher surface area, which exhibited improved electrocatalytic activity for HER in comparison to MOF-free Ni–S [76]. NU-1000 thin films were synthesized on FTO using hydrothermal process, and Ni–S were then fabricated at the end terminals of the NU-1000 nanorods via electrodeposition, leading to the NU-1000/Ni–S composite on electrode surface. By integrating with MOFs, the active surface area of the metal-sulfide based catalyst was enhanced, which improved the catalytic activity. Suh and coworkers have designed CuS NPs within HKUST-1 ( $[\text{Cu}_3(\text{BTC})_2 \cdot (\text{H}_2\text{O})_3]$ ), which showed the excellent ORR activity in an alkaline solution (Fig. 11) [62]. With the increase of Cu–S content in the MOF, the conductivity was found to be enhanced significantly. This new composite material that consists of 28 wt% Cu–S NPs in MOF template showed the onset potential of 0.91 V versus RHE via four electron transfer pathways (Fig. 11b, c). Metal oxide NPs can also be embedded in the MOFs, which can prevent them to aggregate during the chemical processing and hence improve their catalytic activities as well as stability in the framework. Yin and coworkers have prepared a  $\epsilon\text{-MnO}_2$ @Fe-MOF composite, in which nanorod particles of  $\epsilon\text{-MnO}_2$  were embedded separately on the surface of a Fe-MOF template [77]. With improved structural morphology, this  $\epsilon\text{-MnO}_2$ @Fe-MOF composite showed remarkable ORR electrocatalytic activity and good stability in an alkaline solution as compare to the intrinsic  $\epsilon\text{-MnO}_2$ .

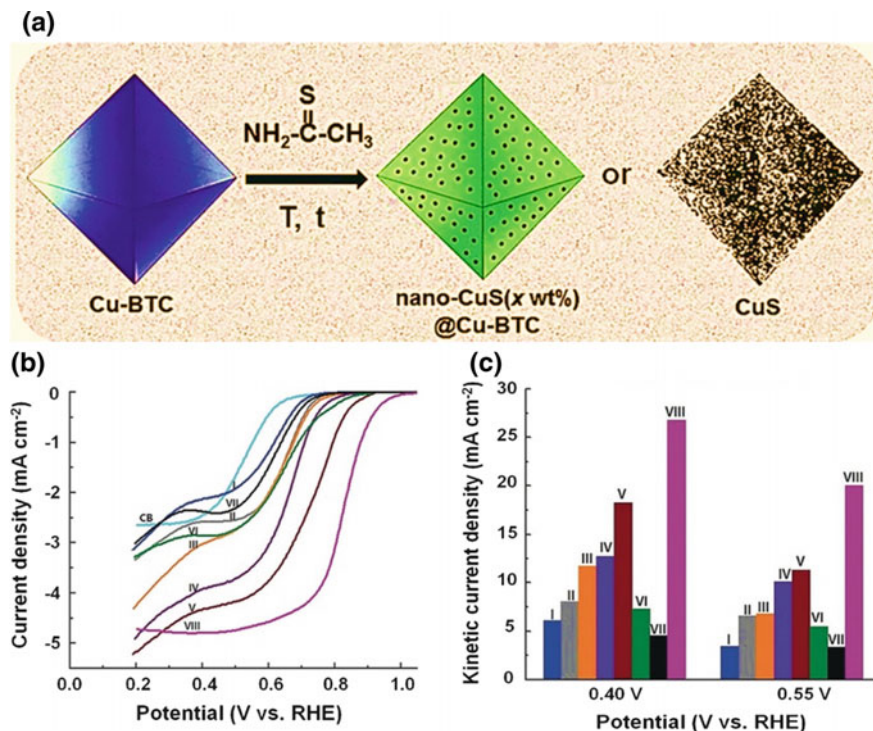


**Fig. 11** a Synthetic scheme of nanosized-CuS( $x$  wt%)@Cu-BTC and nano-CuS(99 wt%). b Linear sweep voltammetry curves for composites I–VIII in 0.1 M KOH at scan rate of  $10 \text{ mV s}^{-1}$ . c Kinetic current density measured at 0.40 and 0.55 V versus RHE. I = Cu-BTC, II = (1.4 wt%) nano-CuS@Cu-BTC, III = (5.3 wt%) nano-CuS@Cu-BTC, IV = (8.8 wt%) nano-CuS@Cu-BTC, V = (28 wt%) nano-CuS@Cu-BTC, VI = (56 wt%) @nano-CuS@Cu-BTC, VII = (99 wt%) nano-CuS and VIII = Pt/C. Reprinted with permission from Ref. [62]. Copyright 2016 John Wiley and Sons

### 2.2.5 MOF Grown on Substrates

Integration of catalytic functional materials into MOFs have been extensively reported with improved catalytic performances. However, for practical applications of MOFs and their composites as electrodes, it is needed to fabricate them in the form of uniform membranes. Uniform growth of MOFs into a thin film can not only improve the charger transfer but also expose more active metal sites, and hence MOFs in form of thin films or sheet could exhibit the better catalytic activity. In this regard, there are few examples, where MOFs have been grown either on a particular substrate or utilized as the self-supported electrode materials for electrocatalysis. In 2016, Tang and coworkers have reported ultrathin nanosheets of NiCo-based bimetallic MOF on the surface of copper foam, which showed improved OER activity due to high conductive nature of copper form as compared to glassy carbon electrodes [78]. Zhao and coworkers have also reported ultrathin MOFs array grown on different

substrates (e.g., nickel foam (NF), glassy carbon (GC), etc.) which displayed good catalytic activities for both the OER and HER [79]. The electrical conductivity of ultrathin MOF nansheets grown on the surface of NF was investigated, which was significantly higher than bulk MOF material and was the main contributor towards high catalytic performance of the ultrathin MOFs array. Recently, Fischer and coworkers have reported the growth of surface-mounted MOF (SURMOF) thin films directly on electrode via layer-by-layer deposition [80]. These SURMOF films and their derivatives (SURMOFD) showed an excellent mass activity of  $2.5 \text{ mA } \mu\text{g}^{-1}$  at  $\eta = 300 \text{ mV}$  for OER with high stability (100 h). The catalytic performance of SURMOFD was found to be highly reliant on thickness and shape of the MOF films. Approach to control the thickness and morphology of self-supported MOF composite electrodes was also reported, where a NiFe alloy foam (NFF) has been used as a substrate as well as metal source (Fig. 12a) [81]. Ni(Fe)-MOF nanosheets with ultralow thickness of  $\sim 1.5 \text{ nm}$  have been constructed on the surface of NFF as self-supported NiFe-NFF electrode, which showed outstanding OER properties with current densities of 10 and  $100 \text{ mA cm}^{-2}$  at overpotentials of 227 and  $253 \text{ mV}$ , respectively (Fig. 12b, c).

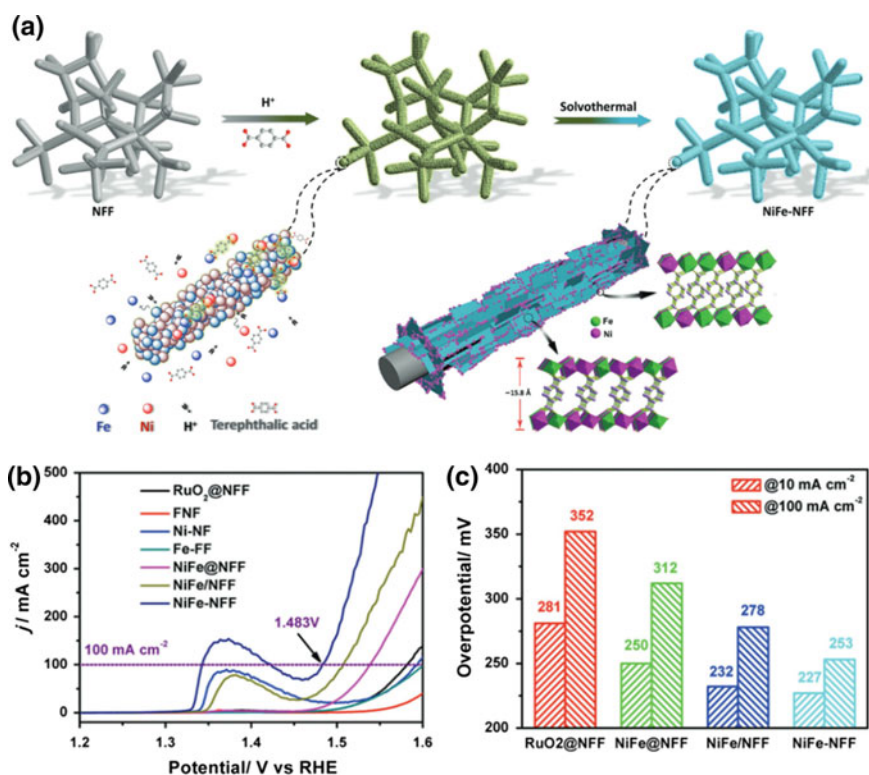


**Fig. 12** **a** Illustration for the preparation of the free-standing NiFe-NFF electrode. **b** LSV plots and **c** the overpotentials and current density relation for the electrodes. Reprinted with permission from Ref. [81]. Copyright 2016 John Wiley and Sons

Outstanding electrocatalytic performance of the NiFe-NFF electrodes was due to the nanoarchitecture of MOF composite, which provided additional active metal sites, Ni and Fe interactions and improved conductivity.

Lu and coworkers have reported a bimetallic MOF, which displayed superior catalytic activity for water splitting after its fabrication on the surface of NF [82]. MIL-53(FeNi) grown on NF have also showed excellent catalytic activity for OER in 1 M KOH with the current density of  $50 \text{ mA cm}^{-2}$  at  $\eta = 233 \text{ mV}$  and Tafel slope =  $31.3 \text{ mV dec}^{-1}$  [83]. The 3D NF is one of the suitable materials for electrocatalysis due to its high porosity, high conductivity and mechanical strength. The growth of MOFs on NF is a quite successful technique to develop binder-free 3D electrodes, which not only increases the charge transfer in MOF/NF, but also improves mechanical stability. Besides, NF provides extra Ni metal center, which increases the number of active metal sites on bimetallic MOFs [83].

In short, the integration of MOFs and other functional materials could combine the characteristics and advantages of them, providing great potential for electrocatalytic applications. A list of different MOF composites for HER, OER and ORR applications is given in Table 2.

### 2.3 MOF-Derived Materials as Electrocatalysts

Although intrinsic MOFs exhibit excellent electrocatalytic activities; however, their low electrical conductivity and poor stability in acidic/basic media prompt researchers to search for alternative routes to use MOFs. Hence, since the first study in the synthesis of porous carbons from MOFs reported by Xu et al. [88], the pyrolysis of MOFs at high temperature provides an effective way to obtain MOF-derived materials for efficient electrocatalytic applications. Generally, two kinds of carbon-based materials, i.e., pure porous carbons and carbon composite materials, can be derived from MOFs depending on pyrolysis conditions. Carbon-based materials derived from MOFs usually have the advantageous features of high porosity and surface areas, appropriate doping of nitrogen and/or metal-based components, more catalytically active sites and efficient electron transfer paths. Numerous MOF-derived materials have been reported for their excellent catalytic performance as electrocatalysts (Table 3). The electrocatalytic properties of MOF-derived materials are highly dependent on the pyrolysis conditions, including heating temperature, holding time, and gas flow etc.

Pyrolysis of ZIF-8, a MOF known for its high thermal stability and surface area, produced a high N-doped carbon material with N of 8.4%, while not compromising on surface area and porosity [89]. Pyrolyzed ZIF-8 showed an excellent HER activity at cathodic polarization treatment for 6 h in 0.5 M  $\text{H}_2\text{SO}_4$  solution. Nano-sized FeCo alloy embedded in N-doped graphene derived from a Co-Fe containing MOF as stable HER catalyst were reported by Chen and coworkers in 2015 [90]. Electrochemical study revealed that this MOF-derived hybrid material displayed the excellent HER activity with an overpotential of  $\eta_{10} = -0.262 \text{ V}$  versus RHE

**Table 2** Examples of MOF composite materials as electrocatalysts for HER, OER and ORR

Catalysts	Short names	Electrochemical reactions (electrolyte)	$\eta_{10}$ (mV) versus RHE	TS (mV dec <sup>-1</sup> )	References
(tba) <sub>3</sub> [(PMo <sub>12</sub> O <sub>36</sub> (OH) <sub>4</sub> Zn <sub>4</sub> )(btc) <sub>4/3</sub> ]	$\epsilon$ (btc) <sub>4/3</sub>	HER (1 M LiCl/HCl)	99 (7 $\mu$ A cm <sup>-2</sup> )	NA	[68]
(tba) <sub>3</sub> [(PMo <sub>12</sub> O <sub>36</sub> (OH) <sub>4</sub> Zn <sub>4</sub> )(btc) <sub>4/3</sub> ]	$\epsilon$ (btc) <sub>4/3</sub>	HER (0.5 M H <sub>2</sub> SO <sub>4</sub> )	515	142	[53]
(tba) <sub>3</sub> [(PMo <sub>12</sub> O <sub>36</sub> (OH) <sub>4</sub> Zn <sub>4</sub> )(btb) <sub>4/3</sub> ]	NENU-500	HER (0.5 M H <sub>2</sub> SO <sub>4</sub> )	237	96	[53]
(tba) <sub>3</sub> [(PMo <sub>12</sub> O <sub>37</sub> (OH) <sub>3</sub> Zn <sub>4</sub> )(bpt)]	NENU-501	HER (0.5 M H <sub>2</sub> SO <sub>4</sub> )	392	137	[53]
(tma) <sub>2</sub> [Cu <sub>2</sub> (btc) <sub>4/3</sub> (H <sub>2</sub> O) <sub>2</sub> ] <sub>6</sub> [HPMo <sub>12</sub> O <sub>40</sub> ]	NENU-5	HER (0.5 M H <sub>2</sub> SO <sub>4</sub> )	858	94	[53]
(tba) <sub>2</sub> [Co(bpy) <sub>3</sub> ] <sub>4</sub> [PMo <sub>12</sub> O <sub>37</sub> (OH) <sub>3</sub> Zn <sub>4</sub> ](btb) <sub>4/3</sub>	[Co- $\epsilon$ (btb) <sub>4/3</sub> ]	HER (0.5 M H <sub>2</sub> SO <sub>4</sub> )	419	NA	[70]
[Ru(bpy) <sub>3</sub> ] <sub>4</sub> [PMo <sub>12</sub> O <sub>38</sub> (OH) <sub>2</sub> Zn <sub>4</sub> ] <sub>2</sub> (btc) <sub>2</sub>	[Ru- $\epsilon$ 2(btc) <sub>2</sub> ]	HER (0.5 M H <sub>2</sub> SO <sub>4</sub> )	617	NA	[70]
[Ru(bpy) <sub>3</sub> ] <sub>3</sub> [PMo <sub>12</sub> O <sub>37</sub> (OH) <sub>3</sub> Zn <sub>4</sub> Cl] <sub>2</sub> (bpdc) <sub>2</sub>	[Ru- $\epsilon$ 2(bpdc) <sub>2</sub> ]	HER (0.5 M H <sub>2</sub> SO <sub>4</sub> )	337	NA	[70]
[Zr <sub>6</sub> ( $\mu$ <sub>3</sub> -OH) <sub>8</sub> (tbapy) <sub>2</sub> ]/Ni-S	NU-1000/Ni-S	HER (0.5 M H <sub>2</sub> SO <sub>4</sub> )	238	182	[76]
(MoS <sub>x</sub> ) <sub>5</sub> /[Zr <sub>6</sub> ( $\mu$ <sub>3</sub> -O) <sub>4</sub> ( $\mu$ <sub>3</sub> -OH) <sub>4</sub> ](anbdc) <sub>6</sub> ]	(MoS <sub>x</sub> ) <sub>5</sub> /UiO-66-NH <sub>2</sub>	HER (0.5 M H <sub>2</sub> SO <sub>4</sub> )	200	59	[64]
GO/[Cu <sub>2</sub> (bdc) <sub>2</sub> (ted) <sub>2</sub> ]	GO/Cu-MOF	HER (0.5 M H <sub>2</sub> SO <sub>4</sub> )	159	84	[71]

(continued)

Table 2 (continued)

Catalysts	Short names	Electrochemical reactions (electrolyte)	$\eta_{10}$ (mV) versus RHE	TS (mV dec <sup>-1</sup> )	References
GO/H <sub>3</sub> [Co <sub>3</sub> (tht)(tha)]	GO/THTA-Co	HER (0.5 M H <sub>2</sub> SO <sub>4</sub> )	230 ± 2.2	70 ± 1.4	[52]
[Fe <sub>1.84</sub> Co <sub>1.16</sub> F(H <sub>2</sub> O) <sub>2</sub> O(btc) <sub>2</sub> ]	Co/MIL-100(Fe)	OER (0.1 M KOH)	734 (5 mA cm <sup>-2</sup> )	NA	[84]
[Zr <sub>6</sub> (μ <sub>3</sub> -O) <sub>8</sub> (μ <sub>3</sub> -OH) <sub>4</sub> ][bpdC] <sub>5.61</sub> [Ru(tpy)(dcipy)(OH <sub>2</sub> ) <sub>0.39</sub> ](ClO <sub>4</sub> ) <sub>0.78</sub>	UiO-67-[RuOH <sub>2</sub> ]	OER (1 M KNO <sub>3</sub> )	818 (0.15 mA cm <sup>-2</sup> )	NA	[65]
[Cr <sub>3</sub> F(H <sub>2</sub> O) <sub>2</sub> O(btc) <sub>2</sub> ]:[Co(salen)]	Co-salen@MIL-100(Cr)	ORR (0.1 M PB)	3.84	NA	[63]
(Co species)@[Cr <sub>3</sub> F(H <sub>2</sub> O) <sub>2</sub> O(bdc) <sub>3</sub> ]	Co/MIL-101(Cr)-R	ORR (0.1 M KOH)	3.9	-107	[85]
G-py/[Zr <sub>6</sub> (μ <sub>3</sub> -OH) <sub>8</sub> (OH) <sub>8</sub> (Fe)(tepp)C <sub>2</sub> ]	G-py/PCN-222	ORR (0.5 M H <sub>2</sub> SO <sub>4</sub> )	NA	NA	[86]
GO(8 wt%)/[Cu <sub>2</sub> (bdc) <sub>2</sub> (ted) <sub>2</sub> ]	GO(8 wt%)/Cu-MOF	ORR (0.5 M H <sub>2</sub> SO <sub>4</sub> )	NA	-69	[71]
ε-MnO <sub>2</sub> /[Fe <sub>3</sub> F(H <sub>2</sub> O) <sub>2</sub> O(btc) <sub>2</sub> ]	ε-MnO <sub>2</sub> /MIL-100(Fe)	ORR (0.1 M KOH)	3.8 (0.55 V)	-117	[77]
CuS(28 wt%)/[Cu <sub>3</sub> (bic) <sub>2</sub> (H <sub>2</sub> O) <sub>3</sub> ]	CuS(28 wt%)/HKUST-1	ORR (0.1 M KOH)	3.82 (0.55 V)	-NA	[62]
rGO/[Cu <sub>2</sub> (tmbdi)(H <sub>2</sub> O) <sub>2</sub> ]	rGO/NPC-4	ORR (0.1 M PB)	1.8 (0.67 V), 3.2 (0.37 V)	NA	[87]

**Table 3** Examples of MOF-derived materials as electrocatalysts for HER, OER and ORR

MOF derivatives	Short names	Electrochemical reactions (electrolyte)	$\eta_{10}$ (mV) versus RHE	TS (mV dec <sup>-1</sup> )	References
CoSe <sub>2</sub> nanoparticles anchored on carbon fibers	ZIF-67	HER (1 M KOH)	95	52	[117]
Hollow CoS <sub>2</sub> nanotube arrays	ZIF-L(Co)	HER (1 M KOH)	193	88	[118]
Ni–Co bimetal phosphide nanotubes	MOF-74	HER (1 M KOH)	129	52	[119]
RuCo@N-doped C	Co <sub>3</sub> [Co(CN) <sub>6</sub> ] <sub>2</sub> Prussian blue analogue	HER (1 M KOH)	28	31	[120]
N-Doped C@Co–N-doped C core–shell nanocages	ZIF-8@ZIF67	OER (0.1 M KOH)	410	91	[121]
Hollow Co <sub>3</sub> O <sub>4</sub> nanospheres in N-doped C	ZIF-L(Co)	OER (1 M KOH)	352	N/A	[122]
Ni–Co bimetal phosphide nanotubes	MOF-74	OER (1 M KOH)	245	61	[119]
Hollow CoS <sub>2</sub> nanotube arrays	ZIF-L(Co)	OER (1 M KOH)	276	81	[118]
CoSe <sub>2</sub> nanoparticles anchored on carbon fibers	ZIF-67	OER (1 M KOH)	297	41	[117]
N-Doped C nanotube frameworks	ZIF-67	OER (0.1 M KOH)	370	93	[123]
N-Doped C nanotube frameworks	ZIF-67	ORR (0.1 M KOH)	N/A	64	[123]
Hollow Co <sub>3</sub> O <sub>4</sub> nanospheres in N-doped C	ZIF-L(Co)	ORR (1 M KOH)	N/A	51	[122]
Co single atoms on N-doped C	Bimetallic Zn/Co-MOF (ZIF-8/67)	ORR (0.1 M KOH)	N/A	75	[124]

(continued)

**Table 3** (continued)

MOF derivatives	Short names	Electrochemical reactions (electrolyte)	$\eta_{10}$ (mV) versus RHE	TS (mV dec <sup>-1</sup> )	References
Honeycomb-like carbon-based framework	CoAl-LDH@ZIF-67	ORR (0.1 M KOH)	N/A	63	[125]
N-Doped C@Co-N-doped C core-shell nanocages	ZIF-8@ZIF67	ORR (0.1 M KOH)	N/A	51	[121]

and high stability even for more than 10000 cycles. Benefited from the high thermal stability, Co-based ZIF-67 is also one of the most commonly used MOFs for preparing various electrocatalysts. Xia and coworkers have also reported the HER catalytic activity of cobalt NPs inserted in a nitrogen-doped carbon material, attained by low-temperature pyrolysis of ZIF-67, with  $\eta_{10} = 0.339$  V versus RHE and Tafel slope = 119 mV dec<sup>-1</sup> [91]. Careful control of the pyrolysis of MOFs can even get the desired catalytic materials with intriguing morphologies. Chen and coworkers reported the carbonization-oxidation-selenylation process of ZIF-67 to design CoSe<sub>2</sub> nanoparticles integrated in defect carbon nanotubes (CoSe<sub>2</sub>@DC), which displayed outstanding HER catalytic performance (Fig. 13) [92].

The pyrolysis of ZIF-67, PEG-2000, urea and boric acid, followed by phosphidation resulted in the formation of CoP@BCN-1 nanotubes, which exhibited excellent

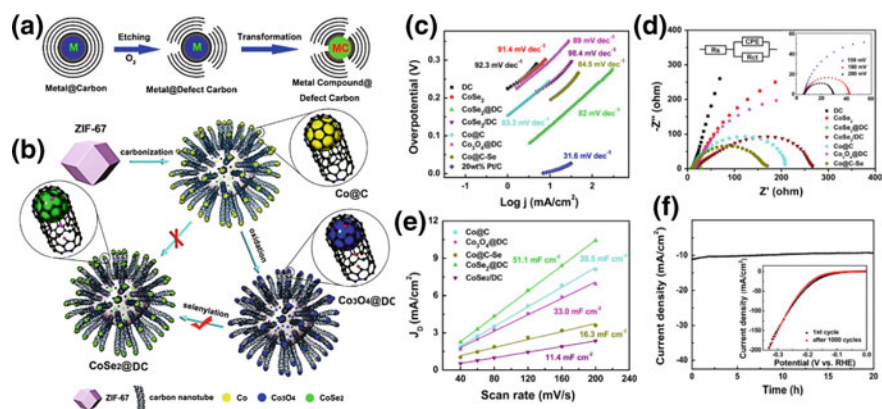


**Fig. 13** a Designing methods for the metal compound @ carbon via oxidation. b Systematic preparation of CoSe<sub>2</sub>@DC. c Tafel plots of inorganic materials and derived materials. d Nyquist plots of the various compounds coated on electrodes (Circuit diagram and Nyquist plots of CoSe<sub>2</sub>@DC-modified electrodes is shown in inset). e Capacitive current versus scan rate. f Chronoamperometric behavior (polarization curves in inset) for CoSe<sub>2</sub>@DC. Reprinted with permission from Ref. [92]. Copyright©2016 Elsevier

electrocatalytic activity for HER in 1 M KOH (alkaline; pH = 13.9), 0.5 M H<sub>2</sub>SO<sub>4</sub> (acidic; pH = 0.3) and 1 M phosphate (neutral; pH = 7) solutions [93]. With more active sites in CoP@BCN-1 nanotubes, ZIF-derived electrocatalysts showed lower overpotentials of 87, 215, and 122 mV in acidic, basic and neutral buffer solutions, respectively. Cobalt-nitrogen-doped graphene aerogel (Co–N–GA) electrocatalyst was also investigated by the pyrolysis of the MOFs@GA composite, which was synthesized by the reaction of Co(ii) ions on graphene oxide (GO) sheets and 5-amino-1*H*-tetrazol [94]. Co–N–GA inherited the highly ordered porosity from MOF, which led to its superior electrocatalytic performance as compared to other non-noble metal HER catalysts.

ZIFs have been extensively utilized for the derivation of carbon-based materials. However, many carboxylate linker-based MOFs have also been pyrolyzed to form metal-doped carbon-based materials. Lee and coworkers have reported the pyrolysis of a 2D sheet structured Co-based MOF and hexamethylenetetramine at 650 °C in argon atmosphere, which resulted in the development of 2D layers of Co/N-carbon [95]. This composite showed quite good HER catalytic performance with a low overpotential of  $\eta_{10} = 103$  mV versus RHE, high-cycle durability and stability. Beside Co-based MOF, Wang and coworkers have investigated a Ni-containing MOF, [Ni<sub>2</sub>(BDC)<sub>2</sub>Ted], to derive carbon materials, which can show electrocatalytic activity for HER [96]. Nanoparticles of Ni with surface nitridation on the carbon sheets derived from the Ni-based MOF were mainly responsible for improving the HER catalytic performance. In a two-step process, N-doped graphene oxide/nickel sulfide (NGO/Ni<sub>7</sub>S<sub>6</sub>) composite nanosheets resulted from the pyrolysis of Ni-MOF-74 possessed highly order porosity, nitrogen contents, accessible nickel active sites, good mass transfer, and high stability against corrosion, showing excellent HER performance [97].

In Sect. 2.2.3, it has been reported that the combination of MOFs and graphene is useful to improve the overall electrical conductivity for prompting their electrocatalytic performance. Alternatively, graphitic carbon with uniform metallic nanoparticles can be obtained upon the pyrolysis of a MOF in an inert atmosphere, which could be used as efficient electrocatalysts [98]. Jiang and coworkers have reported the Ni@graphene derived from a Ni-based MOF, which exhibited tremendous catalytic activity in a 1.0 M KOH solution [99]. This MOF derived Ni-based electrocatalysts with excellent HER as well as ORR performance represents an ideal material to be used for water splitting. ZIF-8 nanocrystals fabricated on GO (ZIF-8@GO) were treated at 900 °C to design N-doped porous carbon@graphene (N-PC@G) with high porosity (1094.3 m<sup>2</sup> g<sup>-1</sup>), micro- and mesopores, appropriate N content, and high degree of graphitization [100]. This N-PC@G-0.02 exhibited tremendous electrocatalytic activity for ORR and high stability.

The conditions of pyrolysis or thermal treatment are significantly important for the final state of the metals in the derived materials and their morphologies. For instance, nanoporous carbon–cobalt oxide hybrids have been reported, which were obtained by the pyrolysis of a cobalt-based ZIF-9 in two-step process as shown in Fig. 14 [101]. The transformation of cobalt to cobalt oxide was highly dependent on the conditions of thermal treatment. Despite the lower surface area, the Z9-800-250

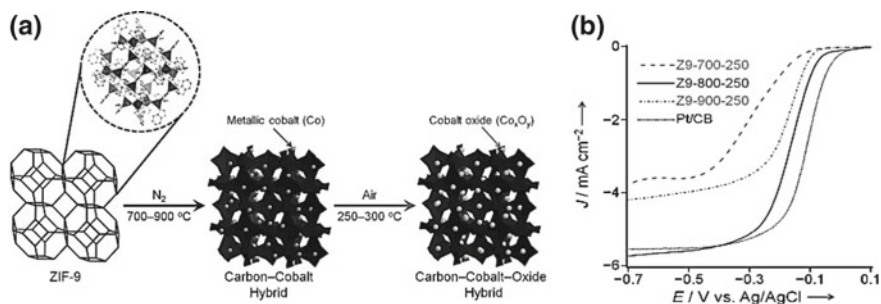


**Fig. 14** **a** Schematic illustrations for the preparation of carbon–cobalt oxide composites via 2-step thermal processing of ZIF-9. **b** Polarization plot for ORR of different electrode materials modified with Z9-900-250, Z9-800-250, Z9-700-250 and Pt/CB at 2000 rpm and  $5 \text{ mV s}^{-1}$ . Reprinted with permission from Ref. [101]. Copyright©2014 John Wiley and Sons

sample exhibited improved electrocatalytic performance for ORR as compared to the Z9-900-250 sample, which is due to better conversion rate of metallic cobalt to cobalt oxide for Z9-800-250. Shape and size of the parental MOFs are also important to get the derived porous materials with desired nanoscale morphologies and optimized functionality. Co NP-contained nitrogen-doped carbon polyhedrons were prepared from ZIF-67, where the derived materials preserved the size and morphology of the parental MOF [102]. The nano-sized MOF derived materials exhibited improved performance towards ORR in acidic solution as compared with those derived from large-sized MOF precursors.

Bimetallic MOFs are also good candidates for the design of high-performance ORR electrocatalysts. The pyrolysis of the Zn–Co bimetallic MOF afforded the Co–N–C electrocatalyst with high porosity ( $\sim 500 \text{ m}^2 \text{ g}^{-1}$ ), orderly-distributed Co NPs ( $\sim 9.5 \text{ nm}$ ), and appropriate N contents (8.5%) [103]. The catalytic properties of this porous Co–N–C polyhedron electrocatalysts have been tested in different buffer solutions and found that it exhibited good catalytic activity and stability, comparable to the well-known commercial ORR catalytic Pt/C, as shown in Fig. 15. MOF-derived Co,N-doped carbons have also been synthesized via a mesoporous silica ( $\text{mSiO}_2$ )-protected calcination method [104]. Zn–Co bimetallic ZIF NPs were coated with  $\text{mSiO}_2$  and treated at  $900 \text{ }^\circ\text{C}$ . Outer coating of mesoporous silica prevented the aggregation of Co,N-doped carbon material particles and the  $\text{mSiO}_2$  was finally removed by chemical wet etching. This MOF-derived material exhibited excellent catalytic activity for ORR in alkaline solution.

Beside metal/metal oxide NP-embedded carbon materials, there are also many reports on the preparation and electrocatalytic properties of MOF-derived metal phosphides, sulfides, and so on. Zhu et al. have constructed the N and S dual-doped honeycomb-like porous carbons immobilizing cobalt sulfide nanoparticles ( $\text{Co}_9\text{S}_8@\text{CNS}$ ) from a MOF, which exhibited excellent catalytic performance for ORR (Fig. 16) [105]. The unique structural and doping properties with increased accessible active sites with synergetic interactions and enhanced mass transport of

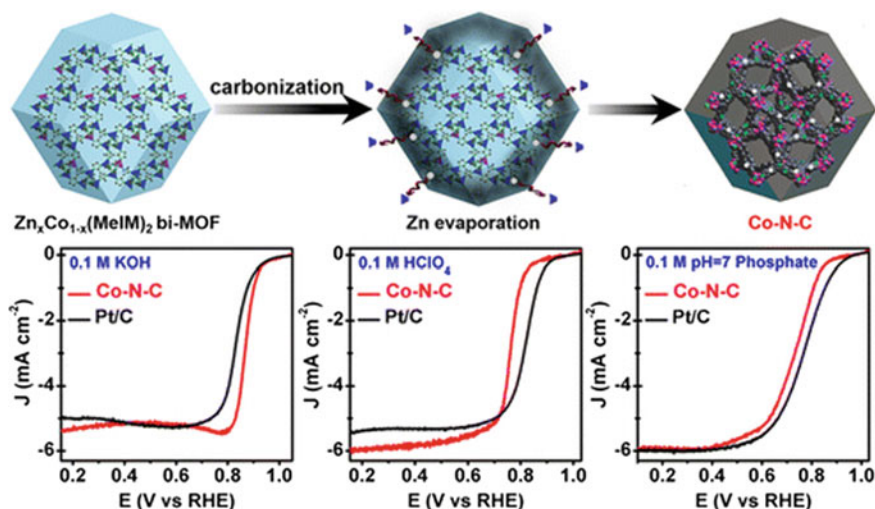


**Fig. 15** Schematic preparation of Co–N–C via carbonization without any post-treatment. MOF-derived Co–N–C exhibited excellent ORR activity that is comparable and much stable than Pt/C in different electrolytes. Reproduced with permission from Ref. [103]. Copyright©2015 American Chemical Society

oxygen and electrolyte in this open nanostructure led to notably superior ORR catalytic activity and long-term stability under alkaline conditions. The pyrolysis of core–shell ZIF-8@ZIF-67 material resulted in the generation of CNTs on the top of a polyhedron, which was further treated by oxidation–phosphidation process to form CoP NPs integrated in N-doped carbon hollow polyhedra (NCNHP) [106]. The resulting CoP/NCNHP was used for water splitting, with excellent bifunctional catalytic properties. Ni–Co–P/C nanoboxes were derived from ZIF-67 following several steps [107]. The reaction of ZIF-67 nanocubes prepared by a surfactant-supported method with Ni(NO<sub>3</sub>)<sub>2</sub> resulted in the formation of Ni–Co LDH on the surface of ZIF-67 nanocubes (ZIF-67@LDH nanoboxes), which were subsequently treated with NaH<sub>2</sub>PO<sub>2</sub> to form Ni–Co P/C catalyst. This bimetallic phosphide catalyst exhibited excellent OER activity. With the advantage of higher contact area on electrode, the nanobox like hollow architectures of bimetallic phosphide derived from MOFs afforded better OER performance as compared with the bulk counterpart. Similarly, mix-metal nanocages (Ni–Co based Prussian blue analogue) have also been derived from MOFs, which possessed huge electrolyte/electrode contact area and hence showed good OER activity [108].

Pyrolysis of MOFs can result in the formation of the derivatives in the form of either single metal atom doped or metal derivative doped carbon materials. Recently, single-atom catalysts have been widely used due to the fine dispersion of single metal active sites. There are several methods to achieve such dispersed single atom active sites on the support materials, such as metals trapped on N-doped carbon materials [109]. Metal nodes and organic linkers are periodically arranged in the

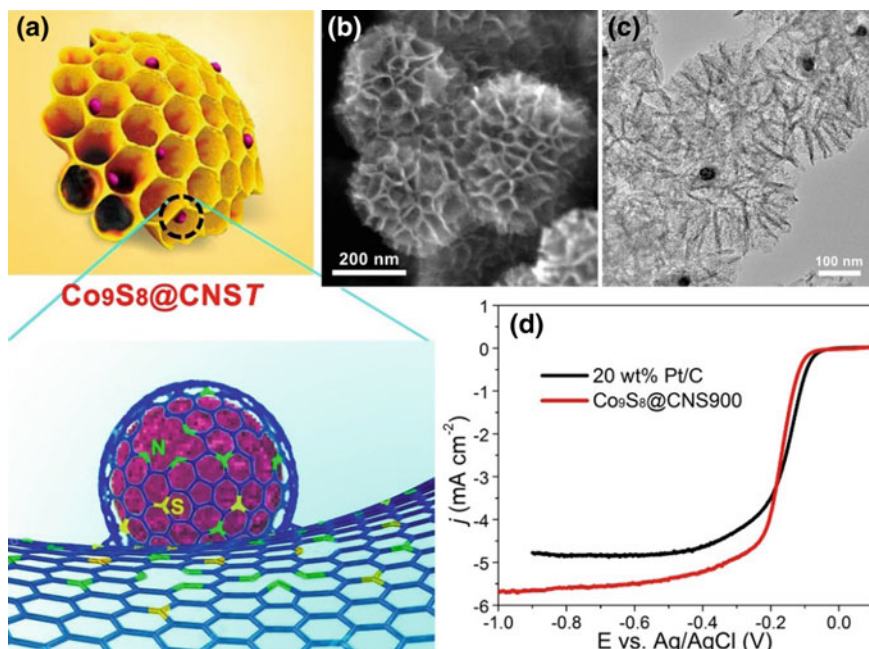


**Fig. 16** **a** Illustration of the honeycomb-like porous structure of Co<sub>9</sub>S<sub>8</sub>@CNS7 catalysts; **b** SEM and **c** TEM images of Co<sub>9</sub>S<sub>8</sub>@CNS900; **d** ORR catalytic properties of Co<sub>9</sub>S<sub>8</sub>@CNS900 and commercial 20 wt% Pt/C catalyst. Reproduced with permission from Ref. [105]. Copyright ©2016 John Wiley and Sons

MOFs, which provides an opportunity to further treat them in order to design such a catalyst, where the active sites are single atomically distributed (called a single metal atom-doped carbon) [110]. Pyrolysis of MOFs can form a single metal atom-doped carbon materials (M–N–C) as excellent catalytic properties [111]. Li and coworkers have synthesized a N-doped single-atom carbon catalyst for ORR, from a bimetallic Zn/Co-based MOF [112]. Addition of Zn ions in precursor resulted in the formation of long-distance dispersion of Co ions, stabilized by N (derived after pyrolysis of MOF). Similarly, a N-doped Fe-single-atom porous catalyst, derived from a MOF composite has also been reported with a unique hierarchical structure having macro-, meso- and microspores [113]. This Fe/N-GPC electrocatalyst was prepared by the pyrolysis of FeD@MIL-101-NH<sub>2</sub> composite and showed outstanding catalytic performance for ORR in alkaline solution, owing to the more accessible active sites and the mass diffusion (Fig. 17). A similar ORR catalyst (Fe/N-GPC) was also designed by the pyrolysis of core-shell Fe(acac)<sub>3</sub>@ZIF-8. Pyrolysis at 800 °C provided the N-doped carbon, while single Fe atoms dispersed on N was achieved from Fe(acac)<sub>3</sub> [114]. A mixed metals based carbon catalyst [CoFe@C], prepared by the one-step pyrolysis of dual metal-doped Zn-MOF, exhibited excellent ORR performance due to periodically dispersion of Co and Fe on porous carbon [115, 116]. Recent studies showed that

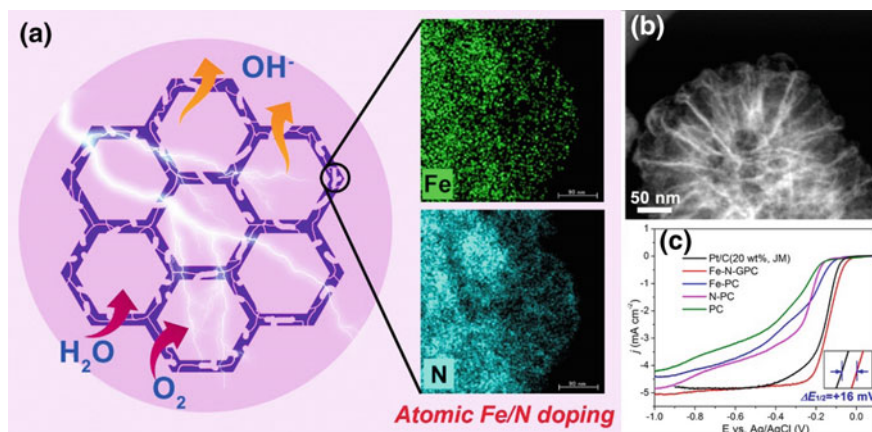


**Fig. 17** **a** Illustration of the hierarchical porous Fe/N-GPC catalysts with atomic Fe and N doping; **b** TEM images of Fe/N-GPC; **c** ORR catalytic properties of Fe/N-GPC, comparative samples and 20 wt% Pt/C catalyst. Reproduced with permission from Ref. [113]. Copyright©2017 American Chemical Society

the single metal atom-doped carbon materials derived from MOFs have significant superior performance as catalysts over traditional metals.

### 3 Conclusion

In this chapter, we have discussed various MOFs, their composites and MOF-derived materials as catalysts various electrochemical reactions, including HER, OER, ORR and other redox reactions. MOFs with their advantageous features such as ultrahigh porosity, large surface areas and structural tunability have significant applications in redox chemistry. However, their low stability and conductivity are the negative factors, which should be controlled in order to improve their electrocatalytic properties. In order to improve the catalytic behaviors, MOFs are composited with conducting materials like graphene, metal NPs, metal oxides/sulfides and so on, which not only enhances their electrical conductivity but also gives additional electrocatalytic features. The unique morphologies and ultrahigh surface areas of MOFs further prompted researchers to pyrolyze them to drive carbon-based materials, which can inherit MOFs' high surface areas and morphologies and perform better electrocatalytic activity and stability than the original MOFs. A series of MOFs, their composites, and MOF-derived materials are discussed here for their electrocatalytic applications. Nonetheless, further investigations are still essential in the field of MOF electrocatalysts. Crystal design and structural morphologies, theoretical simulations, and computational studies should be further performed, which could help to optimize and evaluate their electrochemical properties.

## References

1. Furukawa H, Cordova KE, O'Keeffe M, Yaghi OM (2013) The chemistry and applications of metal-organic frameworks. *Science* 341:1230444
2. Schröder M (2010) *Functional metal-organic frameworks: gas storage, separation and catalysis*, 1st edn. Springer, Berlin
3. Kirchon A, Feng L, Drake HF, Joseph EA, Zhou H-C (2018) From fundamentals to applications: a toolbox for robust and multifunctional MOF materials. *Chem Soc Rev* 47:8611–8638
4. Wang H, Zhu Q-L, Zou R, Xu Q (2017) Metal-organic frameworks for energy applications. *Chem* 2:52–80
5. Zhou HC, Kitagawa S (2014) Metal-organic frameworks (MOFs). *Chem Soc Rev* 43:5415–5418
6. Lu W, Wei Z, Gu Z-Y, Liu T-F, Park J, Park J, Tian J, Zhang M, Zhang Q, Gentle T III, Bosch M, Zhou H-C (2014) Tuning the structure and function of metal-organic frameworks via linker design. *Chem Soc Rev* 43:5561–5593
7. Deria P, Mondloch JE, Karagiari O, Bury W, Hupp JT, Farha OK (2014) Beyond post-synthesis modification: evolution of metal-organic frameworks via building block replacement. *Chem Soc Rev* 43:5896–5912
8. Farha OK, Wilmer CE, Eryazici I, Hauser BG, Parilla PA, O'Neill K, Sarjeant AA, Nguyen ST, Snurr RQ, Hupp JT (2012) Designing higher surface area metal-organic frameworks: are triple bonds better than phenyls? *J Am Chem Soc* 134:9860–9863
9. Hendon CH, Rieth AJ, Korzyński MD, Dincă M (2017) Grand challenges and future opportunities for metal-organic frameworks. *ACS Cent Sci* 3:554–563
10. Farha OK, Eryazici I, Jeong NC, Hauser BG, Wilmer CE, Sarjeant AA, Snurr RQ, Nguyen ST, Yazaydin AO, Hupp JT (2012) Metal-organic framework materials with ultrahigh surface areas: is the sky the limit? *J Am Chem Soc* 134:15016–15021
11. Deng H, Grunder S, Cordova KE, Valente C, Furukawa H, Hmadedh M, Gándara F, Whalley AC, Liu Z, Asahina S, Kazumori H, O'Keeffe M, Terasaki O, Stoddart JF, Yaghi OM (2012) Large-pore apertures in a series of metal-organic frameworks. *Science* 336:1018
12. Silva P, Vilela SMF, Tomé JPC, Almeida Paz FA (2015) Multifunctional metal-organic frameworks: from academia to industrial applications. *Chem Soc Rev* 44:6774–6803
13. Kobayashi Y, Jacobs B, Allendorf MD, Long JR (2010) Conductivity, doping, and redox chemistry of a microporous dithiolene-based metal-organic framework. *Chem Mater* 22:4120–4122
14. Hendon CH, Tiana D, Walsh A (2012) Conductive metal-organic frameworks and networks: fact or fantasy? *Phys Chem Chem Phys* 14:13120–13132
15. Stavila V, Talin AA, Allendorf MD (2014) MOF-based electronic and opto-electronic devices. *Chem Soc Rev* 43:5994–6010
16. Silva CG, Corma A, García H (2010) Metal-organic frameworks as semiconductors. *J Mater Chem* 20:3141–3156
17. Talin AA, Centrone A, Ford AC, Foster ME, Stavila V, Haney P, Kinney RA, Szalai V, El Gabaly F, Yoon HP, Léonard F, Allendorf MD (2014) Tunable electrical conductivity in metal-organic framework thin-film devices. *Science* 343:66
18. Sheberla D, Bachman JC, Elias JS, Sun C-J, Shao-Horn Y, Dincă M (2016) Conductive MOF electrodes for stable supercapacitors with high areal capacitance. *Nat Mater* 16:220
19. Sheberla D, Sun L, Blood-Forsythe MA, Er S, Wade CR, Brozek CK, Aspuru-Guzik A, Dincă M (2014) High electrical conductivity in Ni<sub>3</sub>(2,3,6,7,10,11-hexaiminotriphenylene)<sub>2</sub>, a semiconducting metal-organic graphene analogue. *J Am Chem Soc* 136:8859–8862
20. Miner EM, Fukushima T, Sheberla D, Sun L, Surendranath Y, Dincă M (2016) Electrochemical oxygen reduction catalysed by Ni<sub>3</sub>(hexaiminotriphenylene)<sub>2</sub>. *Nat Commun* 7:10942
21. Pathak A, Shen J-W, Usman M, Wei L-F, Mendiratta S, Chang Y-S, Sainbileg B, Ngue C-M, Chen R-S, Hayashi M, Luo T-T, Chen F-R, Chen K-H, Tseng T-W, Chen L-C, Lu K-L

- (2019) Integration of a  $(-\text{Cu}-\text{S}-)_n$  plane in a metal–organic framework affords high electrical conductivity. *Nat Commun* 10:1721
22. Usman M, Mendiratta S, Lu K-L (2017) Semiconductor metal-organic frameworks: future low-bandgap materials. *Adv Mater* 29:1605071
  23. Sivula K, van de Krol R (2016) Semiconducting materials for photoelectrochemical energy conversion. *Nat Rev Mater* 1:15010
  24. Turner JA (2004) Sustainable hydrogen production. *Science* 305:972
  25. Guan BY, Yu L, Lou XW (2016) A dual-metal–organic-framework derived electrocatalyst for oxygen reduction. *Energy Environ Sci* 9:3092–3096
  26. Petit C, Bandosz TJ (2009) MOF–graphite oxide composites: combining the uniqueness of graphene layers and metal-organic frameworks. *Adv Mater* 21:4753–4757
  27. Dang S, Zhu Q-L, Xu Q (2017) Nanomaterials derived from metal–organic frameworks. *Nat Rev Mater* 3:17075
  28. Xu L, Wang X, Chai L, Li T-T, Hu Y, Qian J, Huang S (2019)  $\text{Co}_3\text{O}_4$ -anchored MWCNTs network derived from metal–organic frameworks as efficient OER electrocatalysts. *Mater Lett*
  29. Zhang H, Hwang S, Wang M, Feng Z, Karakalos S, Luo L, Qiao Z, Xie X, Wang C, Su D, Shao Y, Wu G (2017) Single atomic iron catalysts for oxygen reduction in acidic media: particle size control and thermal activation. *J Am Chem Soc* 139:14143–14149
  30. Zhu Q-L, Xu Q (2014) Metal–organic framework composites. *Chem Soc Rev* 43:5468–5512
  31. Ko M, Mendecki L, Mirica KA (2018) Conductive two-dimensional metal–organic frameworks as multifunctional materials. *Chem Commun* 54:7873–7891
  32. Yang HM, Song XL, Yang TL, Liang ZH, Fan CM, Hao XG (2014) Electrochemical synthesis of flower shaped morphology MOFs in an ionic liquid system and their electrocatalytic application to the hydrogen evolution reaction. *RSC Adv* 4:15720–15726
  33. Gong Y, Hao Z, Meng J, Shi H, Jiang P, Zhang M, Lin J (2014) Two  $\text{Co}^{\text{II}}$  metal-organic frameworks based on a multicarboxylate ligand as electrocatalysts for water splitting. *ChemPlusChem* 79:266–277
  34. Gong Y, Shi H-F, Hao Z, Sun J-L, Lin J-H (2013) Two novel  $\text{Co}(\text{ii})$  coordination polymers based on 1,4-bis(3-pyridylaminomethyl)benzene as electrocatalysts for oxygen evolution from water. *Dalton Trans* 42:12252–12259
  35. Wu Y-P, Zhou W, Zhao J, Dong W-W, Lan Y-Q, Li D-S, Sun C, Bu X (2017) Surfactant-assisted phase-selective synthesis of new cobalt MOFs and their efficient electrocatalytic hydrogen evolution reaction. *Angew Chem Int Ed* 56:13001–13005
  36. Phan A, Doonan CJ, Uribe-Romo FJ, Knobler CB, O’Keeffe M, Yaghi OM (2010) Synthesis, structure, and carbon dioxide capture properties of zeolitic imidazolate frameworks. *Acc Chem Res* 43:58–67
  37. Tao L, Lin C-Y, Dou S, Feng S, Chen D, Liu D, Huo J, Xia Z, Wang S (2017) Creating coordinatively unsaturated metal sites in metal-organic-frameworks as efficient electrocatalysts for the oxygen evolution reaction: insights into the active centers. *Nano Energy* 41:417–425
  38. Wang S, Hou Y, Lin S, Wang X (2014) Water oxidation electrocatalysis by a zeolitic imidazolate framework. *Nanoscale* 6:9930–9934
  39. Wang L, Wu Y, Cao R, Ren L, Chen M, Feng X, Zhou J, Wang B (2016) Fe/Ni metal-organic frameworks and their binder-free thin films for efficient oxygen evolution with low overpotential. *ACS Appl Mater Interfaces* 8:16736–16743
  40. Xue Z, Li Y, Zhang Y, Geng W, Jia B, Tang J, Bao S, Wang H-P, Fan Y, Wei Z-W, Zhang Z, Ke Z, Li G, Su C-Y (2018) Modulating electronic structure of metal-organic framework for efficient electrocatalytic oxygen evolution. *Adv Energy Mater* 8:1801564
  41. Wang X-L, Dong L-Z, Qiao M, Tang Y-J, Liu J, Li Y, Li S-L, Su J-X, Lan Y-Q (2018) Exploring the performance improvement of the oxygen evolution reaction in a stable bimetal-organic framework system. *Angew Chem Int Ed* 57:9660–9664
  42. Zhou W, Huang D-D, Wu Y-P, Zhao J, Wu T, Zhang J, Li D-S, Sun C, Feng P, Bu X (2019) Stable hierarchical bimetal-organic nanostructures as high performance electrocatalysts for the oxygen evolution reaction. *Angew Chem Int Ed* 58:4227–4231

43. Li F-L, Shao Q, Huang X, Lang J-P (2018) Nanoscale trimetallic metal-organic frameworks enable efficient oxygen evolution electrocatalysis. *Angew Chem Int Ed* 57:1888–1892
44. Lu X-F, Liao P-Q, Wang J-W, Wu J-X, Chen X-W, He C-T, Zhang J-P, Li G-R, Chen X-M (2016) An alkaline-stable, metal hydroxide mimicking metal-organic framework for efficient electrocatalytic oxygen evolution. *J Am Chem Soc* 138:8336–8339
45. Mao J, Yang L, Yu P, Wei X, Mao L (2012) Electrocatalytic four-electron reduction of oxygen with Copper (II)-based metal-organic frameworks. *Electrochem Commun* 19:29–31
46. Usov PM, Huffman B, Epley CC, Kessinger MC, Zhu J, Maza WA, Morris AJ (2017) Study of electrocatalytic properties of metal-organic framework PCN-223 for the oxygen reduction reaction. *ACS Appl Mater Interfaces* 9:33539–33543
47. Song G, Wang Z, Wang L, Li G, Huang M, Yin F (2014) Preparation of MOF(Fe) and its catalytic activity for oxygen reduction reaction in an alkaline electrolyte. *Chin J Catal* 35:185–195
48. Albo J, Vallejo D, Beobide G, Castillo O, Castaño P, Irabien A (2017) Copper-based metal-organic porous materials for CO<sub>2</sub> electrocatalytic reduction to alcohols. *ChemSusChem* 10:1100–1109
49. Kornienko N, Zhao Y, Kley CS, Zhu C, Kim D, Lin S, Chang CJ, Yaghi OM, Yang P (2015) Metal-organic frameworks for electrocatalytic reduction of carbon dioxide. *J Am Chem Soc* 137:14129–14135
50. Clough AJ, Yoo JW, Mecklenburg MH, Marinescu SC (2015) Two-dimensional metal-organic surfaces for efficient hydrogen evolution from water. *J Am Chem Soc* 137:118–121
51. Dong R, Pfeiffermann M, Liang H, Zheng Z, Zhu X, Zhang J, Feng X (2015) Large-area, free-standing, two-dimensional supramolecular polymer single-layer sheets for highly efficient electrocatalytic hydrogen evolution. *Angew Chem Int Ed* 54:12058–12063
52. Dong R, Zheng Z, Tranca DC, Zhang J, Chandrasekhar N, Liu S, Zhuang X, Seifert G, Feng X (2017) Immobilizing molecular metal dithiolene–diamine complexes on 2D metal–organic frameworks for electrocatalytic H<sub>2</sub> production. *Chem-A Eur J* 23:2255–2260
53. Qin J-S, Du D-Y, Guan W, Bo X-J, Li Y-F, Guo L-P, Su Z-M, Wang Y-Y, Lan Y-Q, Zhou H-C (2015) Ultrastable polymolybdate-based metal-organic frameworks as highly active electrocatalysts for hydrogen generation from water. *J Am Chem Soc* 137:7169–7177
54. Jiang J, Huang L, Liu X, Ai L (2017) Bioinspired cobalt-citrate metal–organic framework as an efficient electrocatalyst for water oxidation. *ACS Appl Mater Interfaces* 9:7193–7201
55. Zhao L, Dong B, Li S, Zhou L, Lai L, Wang Z, Zhao S, Han M, Gao K, Lu M, Xie X, Chen B, Liu Z, Wang X, Zhang H, Li H, Liu J, Zhang H, Huang X, Huang W (2017) Interdiffusion reaction-assisted hybridization of two-dimensional metal-organic frameworks and Ti<sub>3</sub>C<sub>2</sub>T<sub>x</sub> nanosheets for electrocatalytic oxygen evolution. *ACS Nano* 11:5800–5807
56. Xu Q, Li H, Yue F, Chi L, Wang J (2016) Nanoscale cobalt metal–organic framework as a catalyst for visible light-driven and electrocatalytic water oxidation. *New J Chem* 40:3032–3035
57. Wang H, Yin F-X, Chen B-H, He X-B, Lv P-L, Ye C-Y, Liu D-J (2017) ZIF-67 incorporated with carbon derived from pomelo peels: a highly efficient bifunctional catalyst for oxygen reduction/evolution reactions. *Appl Catal B* 205:55–67
58. Shen J-Q, Liao P-Q, Zhou D-D, He C-T, Wu J-X, Zhang W-X, Zhang J-P, Chen X-M (2017) Modular and stepwise synthesis of a hybrid metal-organic framework for efficient electrocatalytic oxygen evolution. *J Am Chem Soc* 139:1778–1781
59. Gong Y, Shi H-F, Jiang P-G, Hua W, Lin J-H (2014) Metal(II)-induced coordination polymer based on 4-(5-(Pyridin-4-yl)-4H-1,2,4-triazol-3-yl)benzoate as an electrocatalyst for water splitting. *Cryst Growth Des* 14:649–657
60. Dai F, Fan W, Bi J, Jiang P, Liu D, Zhang X, Lin H, Gong C, Wang R, Zhang L, Sun D (2016) A lead–porphyrin metal–organic framework: gas adsorption properties and electrocatalytic activity for water oxidation. *Dalton Trans* 45:61–65
61. Lions M, Tommasino JB, Chattot R, Abeykoon B, Guillou N, Devic T, Demessence A, Cardenas L, Maillard F, Fateeva A (2017) Insights into the mechanism of electrocatalysis of the oxygen reduction reaction by a porphyrinic metal organic framework. *Chem Commun* 53:6496–6499

62. Cho K, Han S-H, Suh MP (2016) Copper-organic framework fabricated with CuS nanoparticles: synthesis, electrical conductivity, and electrocatalytic activities for oxygen reduction reaction. *Angew Chem Int Ed* 55:15301–15305
63. Miao P, Li G, Zhang G, Lu H (2014) Co(II)-salen complex encapsulated into MIL-100(Cr) for electrocatalytic reduction of oxygen. *J Energy Chem* 23:507–512
64. Dai X, Liu M, Li Z, Jin A, Ma Y, Huang X, Sun H, Wang H, Zhang X (2016) Molybdenum polysulfide anchored on porous Zr-metal organic framework to enhance the performance of hydrogen evolution reaction. *J Phys Chem C* 120:12539–12548
65. Johnson BA, Bhunia A, Ott S (2017) Electrocatalytic water oxidation by a molecular catalyst incorporated into a metal–organic framework thin film. *Dalton Trans* 46:1382–1388
66. Lin S, Pineda-Galvan Y, Maza WA, Epley CC, Zhu J, Kessinger MC, Pushkar Y, Morris AJ (2017) Electrochemical water oxidation by a catalyst-modified metal-organic framework thin film. *ChemSusChem* 10:514–522
67. Khan MI, Swenson LS (2013) Open-framework hybrid materials and composites from polyoxometalates (Chap. 2). In: *New and future developments in catalysis*. Elsevier Science
68. Nohra B, El Moll H, Rodriguez Albelo LM, Mialane P, Marrot J, Mellot-Drazniaks C, O’Keeffe M, Ngo Biboum R, Lemaire J, Keita B, Nadjo L, Dolbecq A (2011) Polyoxometalate-based metal organic frameworks (POMOFs): structural trends, energetics, and high electrocatalytic efficiency for hydrogen evolution reaction. *J Am Chem Soc* 133:13363–13374
69. Du D-Y, Qin J-S, Li S-L, Su Z-M, Lan Y-Q (2014) Recent advances in porous polyoxometalate-based metal–organic framework materials. *Chem Soc Rev* 43:4615–4632
70. Salomon W, Paille G, Gomez-Mingot M, Mialane P, Marrot J, Roch-Marchal C, Nocton G, Mellot-Drazniaks C, Fontecave M, Dolbecq A (2017) Effect of cations on the structure and electrocatalytic response of polyoxometalate-based coordination polymers. *Cryst Growth Des* 17:1600–1609
71. Jahan M, Liu Z, Loh KP (2013) A graphene oxide and copper-centered metal organic framework composite as a tri-functional catalyst for HER, OER, and ORR. *Adv Funct Mater* 23:5363–5372
72. Nie Y, Li L, Wei Z (2015) Recent advancements in Pt and Pt-free catalysts for oxygen reduction reaction. *Chem Soc Rev* 44:2168–2201
73. Zhu Q-L, Li J, Xu Q (2013) Immobilizing metal nanoparticles to metal-organic frameworks with size and location control for optimizing catalytic performance. *J Am Chem Soc* 135:10210–10213
74. Zhu Q-L, Xu Q (2016) Immobilization of ultrafine metal nanoparticles to high-surface-area materials and their catalytic applications. *Chem* 1:220–245
75. Guo J, Zhang X, Sun Y, Tang L, Liu Q, Zhang X (2017) Loading Pt nanoparticles on metal-organic frameworks for improved oxygen evolution. *ACS Sustain Chem Eng* 5:11577–11583
76. Hod I, Deria P, Bury W, Mondloch JE, Kung C-W, So M, Sampson MD, Peters AW, Kubiak CP, Farha OK, Hupp JT (2015) A porous proton-relaying metal-organic framework material that accelerates electrochemical hydrogen evolution. *Nat Commun* 6:8304
77. Wang H, Yin F, Chen B, Li G (2015) Synthesis of an  $\epsilon$ -MnO<sub>2</sub>/metal–organic-framework composite and its electrocatalysis towards oxygen reduction reaction in an alkaline electrolyte. *J Mater Chem A* 3:16168–16176
78. Zhao S, Wang Y, Dong J, He C-T, Yin H, An P, Zhao K, Zhang X, Gao C, Zhang L, Lv J, Wang J, Zhang J, Khattak AM, Khan NA, Wei Z, Zhang J, Liu S, Zhao H, Tang Z (2016) Ultrathin metal–organic framework nanosheets for electrocatalytic oxygen evolution. *Nat Energy* 1:16184
79. Duan J, Chen S, Zhao C (2017) Ultrathin metal-organic framework array for efficient electrocatalytic water splitting. *Nat Commun* 8:15341
80. Li W, Watzel S, El-Sayed HA, Liang Y, Kieslich G, Bandarenka AS, Rodewald K, Rieger B, Fischer RA (2019) Unprecedented high oxygen evolution activity of electrocatalysts derived from surface-mounted metal-organic frameworks. *J Am Chem Soc* 141:5926–5933

81. Cao C, Ma D-D, Xu Q, Wu X-T, Zhu Q-L (2019) Semisacrificial template growth of self-supporting MOF nanocomposite electrode for efficient electrocatalytic water oxidation. *Adv Funct Mater* 29:1807418
82. Senthil Raja D, Chuah X-F, Lu S-Y (2018) In situ grown bimetallic MOF-based composite as highly efficient bifunctional electrocatalyst for overall water splitting with ultrastability at high current densities. *Adv Energy Mater* 8:1801065
83. Sun F, Wang G, Ding Y, Wang C, Yuan B, Lin Y (2018) NiFe-based metal-organic framework nanosheets directly supported on nickel foam acting as robust electrodes for electrochemical oxygen evolution reaction. *Adv Energy Mater* 8:1800584
84. Wang H, Yin F, Li G, Chen B, Wang Z (2014) Preparation, characterization and bifunctional catalytic properties of MOF(Fe/Co) catalyst for oxygen reduction/evolution reactions in alkaline electrolyte. *Int J Hydrogen Energy* 39:16179–16186
85. He X, Yin F, Li G (2015) A Co/metal-organic-framework bifunctional electrocatalyst: the effect of the surface cobalt oxidation state on oxygen evolution/reduction reactions in an alkaline electrolyte. *Int J Hydrogen Energy* 40:9713–9722
86. Sohrabi S, Dehghanpour S, Ghalkhani M (2016) Three-dimensional metal-organic framework graphene nanocomposite as a highly efficient and stable electrocatalyst for the oxygen reduction reaction in acidic media. *ChemCatChem* 8:2356–2366
87. Jiang M, Li L, Zhu D, Zhang H, Zhao X (2014) Oxygen reduction in the nanocage of metal-organic frameworks with an electron transfer mediator. *J Mater Chem A* 2:5323–5329
88. Liu B, Shioyama H, Akita T, Xu Q (2008) Metal-organic framework as a template for porous carbon synthesis. *J Am Chem Soc* 130:5390–5391
89. Lei Y, Wei L, Zhai S, Wang Y, Karahan HE, Chen X, Zhou Z, Wang C, Sui X, Chen Y (2018) Metal-free bifunctional carbon electrocatalysts derived from zeolitic imidazolate frameworks for efficient water splitting. *Mater Chem Front* 2:102–111
90. Yang Y, Lun Z, Xia G, Zheng F, He M, Chen Q (2015) Non-precious alloy encapsulated in nitrogen-doped graphene layers derived from MOFs as an active and durable hydrogen evolution reaction catalyst. *Energy Environ Sci* 8:3563–3571
91. Zheng F, Xia H, Xu S, Wang R, Zhang Y (2016) Facile synthesis of MOF-derived ultrafine Co nanocrystals embedded in a nitrogen-doped carbon matrix for the hydrogen evolution reaction. *RSC Adv* 6:71767–71772
92. Zhou W, Lu J, Zhou K, Yang L, Ke Y, Tang Z, Chen S (2016) CoSe<sub>2</sub> nanoparticles embedded defective carbon nanotubes derived from MOFs as efficient electrocatalyst for hydrogen evolution reaction. *Nano Energy* 28:143–150
93. Tabassum H, Guo W, Meng W, Mahmood A, Zhao R, Wang Q, Zou R (2017) Metal-organic frameworks derived cobalt phosphide architecture encapsulated into B/N Co-doped graphene nanotubes for all pH value electrochemical hydrogen evolution. *Adv Energy Mater* 7:1601671
94. Zhu Z, Yang Y, Guan Y, Xue J, Cui L (2016) Construction of a cobalt-embedded nitrogen-doped carbon material with the desired porosity derived from the confined growth of MOFs within graphene aerogels as a superior catalyst towards HER and ORR. *J Mater Chem A* 4:15536–15545
95. Huang T, Chen Y, Lee J-M (2017) Two-dimensional cobalt/N-doped carbon hybrid structure derived from metal-organic frameworks as efficient electrocatalysts for hydrogen evolution. *ACS Sustain Chem Eng* 5:5646–5650
96. Wang T, Zhou Q, Wang X, Zheng J, Li X (2015) MOF-derived surface modified Ni nanoparticles as an efficient catalyst for the hydrogen evolution reaction. *J Mater Chem A* 3:16435–16439
97. Jayaramulu K, Masa J, Tomanec O, Peeters D, Ranc V, Schneemann A, Zboril R, Schuhmann W, Fischer RA (2017) Electrocatalysis: nanoporous nitrogen-doped graphene oxide/nickel sulfide composite sheets derived from a metal-organic framework as an efficient electrocatalyst for hydrogen and oxygen evolution. *Adv Funct Mater* 27:1700451
98. Higgins D, Zamani P, Yu A, Chen Z (2016) The application of graphene and its composites in oxygen reduction electrocatalysis: a perspective and review of recent progress. *Energy Environ Sci* 9:357–390

99. Ai L, Tian T, Jiang J (2017) Ultrathin graphene layers encapsulating nickel nanoparticles derived metal-organic frameworks for highly efficient electrocatalytic hydrogen and oxygen evolution reactions. *ACS Sustain Chem Eng* 5:4771–4777
100. Liu S, Zhang H, Zhao Q, Zhang X, Liu R, Ge X, Wang G, Zhao H, Cai W (2016) Metal-organic framework derived nitrogen-doped porous carbon@graphene sandwich-like structured composites as bifunctional electrocatalysts for oxygen reduction and evolution reactions. *Carbon* 106:74–83
101. Chaikittisilp W, Torad NL, Li C, Imura M, Suzuki N, Ishihara S, Ariga K, Yamauchi Y (2014) Synthesis of nanoporous carbon–cobalt-oxide hybrid electrocatalysts by thermal conversion of metal–organic frameworks. *Chem A Eur J* 20:4217–4221
102. Xia W, Zhu J, Guo W, An L, Xia D, Zou R (2014) Well-defined carbon polyhedrons prepared from nano metal–organic frameworks for oxygen reduction. *J Mater Chem A* 2:11606–11613
103. You B, Jiang N, Sheng M, Drisdell WS, Yano J, Sun Y (2015) Bimetal-organic framework self-adjusted synthesis of support-free nonprecious electrocatalysts for efficient oxygen reduction. *ACS Catal* 5:7068–7076
104. Shang L, Yu H, Huang X, Bian T, Shi R, Zhao Y, Waterhouse GIN, Wu L-Z, Tung C-H, Zhang T (2016) Well-dispersed ZIF-derived Co, N-Co-doped carbon nanoframes through mesoporous-silica-protected calcination as efficient oxygen reduction electrocatalysts. *Adv Mater* 28:1668–1674
105. Zhu Q-L, Xia W, Akita T, Zou R, Xu Q (2016) Metal-organic framework-derived honeycomb-like open porous nanostructures as precious-metal-free catalysts for highly efficient oxygen electroreduction. *Adv Mater* 28:6391–6398
106. Pan Y, Sun K, Liu S, Cao X, Wu K, Cheong W-C, Chen Z, Wang Y, Li Y, Liu Y, Wang D, Peng Q, Chen C, Li Y (2018) Core-shell ZIF-8@ZIF-67-derived CoP nanoparticle-embedded N-doped carbon nanotube hollow polyhedron for efficient overall water splitting. *J Am Chem Soc* 140:2610–2618
107. He P, Yu X-Y, Lou XW (2017) Carbon-incorporated nickel-cobalt mixed metal phosphide nanoboxes with enhanced electrocatalytic activity for oxygen evolution. *Angew Chem Int Ed* 56:3897–3900
108. Han L, Yu X-Y, Lou XW (2016) Formation of Prussian-blue-analog nanocages via a direct etching method and their conversion into Ni–Co-mixed oxide for enhanced oxygen evolution. *Adv Mater* 28:4601–4605
109. Qu Y, Li Z, Chen W, Lin Y, Yuan T, Yang Z, Zhao C, Wang J, Zhao C, Wang X, Zhou F, Zhuang Z, Wu Y, Li Y (2018) Direct transformation of bulk copper into copper single sites via emitting and trapping of atoms. *Nat Catal* 1:781–786
110. Wang X, Chen W, Zhang L, Yao T, Liu W, Lin Y, Ju H, Dong J, Zheng L, Yan W, Zheng X, Li Z, Wang X, Yang J, He D, Wang Y, Deng Z, Wu Y, Li Y (2017) Uncoordinated amine groups of metal-organic frameworks to anchor single Ru sites as chemoselective catalysts toward the hydrogenation of quinoline. *J Am Chem Soc* 139:9419–9422
111. Yang Q, Yang C-C, Lin C-H, Jiang H-L (2019) Metal–organic-framework-derived hollow N-doped porous carbon with ultrahigh concentrations of single Zn atoms for efficient carbon dioxide conversion. *Angew Chem Int Ed* 58:3511–3515
112. Ma S, Goenaga GA, Call AV, Liu D-J (2011) Cobalt imidazolate framework as precursor for oxygen reduction reaction electrocatalysts. *Chem A Eur J* 17:2063–2067
113. Zhu Q-L, Xia W, Zheng L-R, Zou R, Liu Z, Xu Q (2017) Atomically dispersed Fe/N-doped hierarchical carbon architectures derived from a metal-organic framework composite for extremely efficient electrocatalysis. *ACS Energy Lett* 2:504–511
114. Chen Y, Ji S, Wang Y, Dong J, Chen W, Li Z, Shen R, Zheng L, Zhuang Z, Wang D, Li Y (2017) Isolated single iron atoms anchored on N-doped porous carbon as an efficient electrocatalyst for the oxygen reduction reaction. *Angew Chem Int Ed* 56:6937–6941
115. Zhao R, Liang Z, Gao S, Yang C, Zhu B, Zhao J, Qu C, Zou R, Xu Q (2019) Puffing up energetic metal-organic frameworks to large carbon networks with hierarchical porosity and atomically dispersed metal sites. *Angew Chem Int Ed* 58:1975–1979

116. Wang J, Huang Z, Liu W, Chang C, Tang H, Li Z, Chen W, Jia C, Yao T, Wei S, Wu Y, Li Y (2017) Design of N-coordinated dual-metal sites: a stable and active Pt-free catalyst for acidic oxygen reduction reaction. *J Am Chem Soc* 139:17281–17284
117. Sun C, Dong Q, Yang J, Dai Z, Lin J, Chen P, Huang W, Dong X (2016) Metal–organic framework derived CoSe<sub>2</sub> nanoparticles anchored on carbon fibers as bifunctional electrocatalysts for efficient overall water splitting. *Nano Res* 9:2234–2243
118. Guan C, Liu X, Elshahawy AM, Zhang H, Wu H, Pennycook SJ, Wang J (2017) Metal–organic framework derived hollow CoS<sub>2</sub> nanotube arrays: an efficient bifunctional electrocatalyst for overall water splitting. *Nanoscale Horiz* 2:342–348
119. Yan L, Cao L, Dai P, Gu X, Liu D, Li L, Wang Y, Zhao X (2017) Metal-organic frameworks derived nanotube of nickel-cobalt bimetal phosphides as highly efficient electrocatalysts for overall water splitting. *Adv Funct Mater* 27:1703455
120. Su J, Yang Y, Xia G, Chen J, Jiang P, Chen Q (2017) Ruthenium-cobalt nanoalloys encapsulated in nitrogen-doped graphene as active electrocatalysts for producing hydrogen in alkaline media. *Nat Commun* 8:14969
121. Liu S, Wang Z, Zhou S, Yu F, Yu M, Chiang C-Y, Zhou W, Zhao J, Qiu J (2017) Metal–organic-framework-derived hybrid carbon nanocages as a bifunctional electrocatalyst for oxygen reduction and evolution. *Adv Mater* 29:1700874
122. Guan C, Sumboja A, Wu H, Ren W, Liu X, Zhang H, Liu Z, Cheng C, Pennycook SJ, Wang J (2017) Hollow Co<sub>3</sub>O<sub>4</sub> nanosphere embedded in carbon arrays for stable and flexible solid-state zinc-air batteries. *Adv Mater* 29:1704117
123. Xia BY, Yan Y, Li N, Wu HB, Lou XW, Wang X (2016) A metal–organic framework-derived bifunctional oxygen electrocatalyst. *Nat Energy* 1:15006
124. Li W-J, Liu J, Sun Z-H, Liu T-F, Lü J, Gao S-Y, He C, Cao R, Luo J-H (2016) Integration of metal-organic frameworks into an electrochemical dielectric thin film for electronic applications. *Nat Commun* 7:11830
125. Li Z, Shao M, Zhou L, Zhang R, Zhang C, Wei M, Evans DG, Duan X (2016) Directed growth of metal-organic frameworks and their derived carbon-based network for efficient electrocatalytic oxygen reduction. *Adv Mater* 28:2337–2344